Available online at www.sciencedirect.com
ScienceDirect
Coordination Chemistry Reviews 251 (2007) 258–287
COORDINATION CHEMISTRY REVIEWS
www.elsevier.com/locate/ccr

Review

Modeling of charge-transfer transitions and excited states in d^6 transition metal complexes by DFT techniques

Antonín Vlček Jr. [a,b,*], Stanislav Záliš [b,**]

[a] *School of Biological and Chemical Sciences, Queen Mary, University of London, Mile End Road, London E1 4NS, United Kingdom*
[b] *J. Heyrovský Institute of Physical Chemistry, Academy of Sciences of the Czech Republic, Dolejškova 3, CZ-182 23 Prague, Czech Republic*

Received 11 February 2006; accepted 18 May 2006
Available online 6 June 2006

Contents

Abbreviations: acac, acetylacetonate; AIM, atoms in molecule; bpy, 2,2′-bipyridine; bza, benzoylacetonate; CASPT2, complete active space with second-order perturbation theory; CASSCF, complete active-space self-consistent field; CC, coupled clusters; COSMO, conductor-like screening model; CPCM conductor-like polarizable continuum model; CT, charge transfer; dab, 1,4-diazabutadiene; DFT, density functional theory; dppz, dipyrido[2,3-a:3′,2′-c]phenazine; en, 1,2-ethylenediamine; GGA, generalized gradient approximation; ILCT, intraligand charge transfer; ISC, intersystem crossing; KS, Kohn–Sham; LCAO, linear combination of atomic orbitals; LF, ligand field (transitions); also called dd; LDA, local density approximation; LLCT, ligand to ligand charge transfer; MD, molecular dynamics; MLCT, metal to ligand charge transfer; MLLCT, metal–ligand-to-ligand charge transfer; MPCT, metal to particle charge transfer; MR-CCI, multireference contracted configuration interaction; MRCI, multireference configuration interaction; MS-CASPT2, multistate CASPT2; NTO, natural transition orbital; OLED, organic light-emitting diode; phen, 1,10-phenanthroline; ppy, 2-phenylpyridine; ppz, 1-phenylpyrazolyl; SAC-CI symmetry-adapted cluster-configuration interaction; TD-DFT, time-dependent DFT; tppz, tetra-2-pyridyl-1,4-pyrazine; tpy, terpyridine; TRIR, time-resolved IR spectroscopy; TR^3, time-resolved resonance Raman; *t*-stpy, *trans*-styrylpyridine; UKS, unrestricted Kohn–Sham; ZINDO, Zerner intermediate neglect of differential overlap

* Corresponding author. Tel.: +44 2078823260; fax: +44 2078827427.
** Corresponding author. Tel.: +420 266053268; fax: +420 286582307.
E-mail addresses: a.vlcek@qmul.ac.uk (A. Vlček Jr.), zalis@jh-inst.cas.cz (S. Záliš).

doi:10.1016/j.ccr.2006.05.021

Abstract

The state of art of the DFT description of charge-transfer electronic excited states of (mostly) d^6 transition metal complexes is presented and discussed. A brief theoretical background places DFT amongst quantum-chemical techniques and discusses the approximations involved. The time-dependent DFT (TD-DFT) treatment of electronic transitions is introduced, with emphasis on the challenges presented by long-range charge separation. Various ways how to characterize excited states in chemically relevant terms are discussed. Several detailed case studies demonstrate how DFT describes charge-transfer excited states of Re^I or Ru^{II} carbonyl-diimine complexes and interprets their photophysics and photochemistry. This "tutorial" section is followed by an overview of DFT and TD-DFT applications to electronic spectroscopy and excited-state properties of metal carbonyls, strongly emissive organometallics, Ru^{II} photosensitizers, luminescent "light-switches" and isonitrile complexes of Re^I and Ru^{II}. Effects of the computational procedure on the quality of the results and the type of information obtained are emphasized. It follows that the most accurate charge-transfer transition energies and descriptions of excited states of low-valent d^6 metal complexes are obtained when using hybrid functionals and calculating the molecule in the actual solvent. A rather delocalized picture of charge-transfer states of these complexes emerges, whereby the electron density is excited from the metal atom and part of its coordination sphere to the electron-accepting ligand.

Keywords: Charge-transfer transition; DFT technique; Re^I and Ru^{II} carbonyl-diimine complex; Excited states; Spectroscopy; Photophysics

1. Introduction

Beautiful colors and rich excited-state behavior are prominent features of transition metal chemistry. Understanding the structure and dynamics of electronic excited states of coordination and organometallic compounds is an important goal of current spectroscopic, photophysical, photochemical and theoretical research [1]. Besides their fundamental importance, these studies are increasingly driven by applications of transition-metal compounds as sensitizers of solar-energy conversion, phosphorescent dyes for display applications (organic light-emitting diodes, OLED), luminescence-based sensors, active components of electron- or energy-transfer assemblies, molecular devices (molectronics), non-linear optical materials, photoinitiators, triggers of electron transfer in biomolecules, or photocatalysts.

In particular, we need to understand the redistribution of electron density brought about by optical excitation and the ensuing structural response of both the excited molecule and its immediate environment. This task is rather challenging for transition-metal compounds due to the simultaneous occurrence of different electronic states in a narrow energy range, strong spin-orbit coupling, long-range charge separation, strong interactions with the medium, or very fast intersystem crossing to triplet states. Despite the very active research in this field, many open questions persist. This is best demonstrated by the most studied inorganic photosensitizer $[Ru(bpy)_3]^{2+}$, whose excited-state electronic structure remains controversial even after more than 20 years of investigations, which have been employing the most advanced spectroscopic techniques.

The interrelated problems of characterization of excited-states and understanding their dynamics can be addressed by combining experimental and theoretical approaches. Electronic absorption spectra in UV–vis or NIR spectral regions provide information on energies and intensities of allowed electronic transitions. Qualitative information on the characters of optically populated (Franck–Condon) excited states can be inferred from solvatochromism or, more precisely, from resonance Raman spectra. Femtosecond rates of ISC to lower-lying triplet states usually prevent detection of the Franck–Condon states by time-resolved spectroscopic techniques, although prompt fluorescence from ^{1}MLCT has been observed for several Ru^{II}, Cu^I and Pt^0 complexes, usually using femtosecond up-conversion [2–6]. Time-resolved laser spectroscopic techniques [7] provide information mostly on low-lying triplet states. In particular, time-resolved UV–vis absorption spectra are an excellent source of kinetic data but reveal less structural information. Time-resolved IR absorption (TRIR) and resonance Raman (TR^3) spectroscopy are more informative in this respect since they interrogate changes of molecular vibrational frequencies upon excitation [7–10]. Recently developed two-dimensional TRIR techniques allow us to track changes in the composition of vibrational normal modes and their coupling after excitation [11,12]. Time-resolved X-ray absorption near-edge structure (XANES) and extended X-ray absorption fine structure (EXAFS) can determine changes in metal–ligand bond lengths and coordination numbers upon electronic excitation. Encouraging results have been obtained on several Ru^{II}, Cu^I or Ni^{II} systems, demonstrating the great potential of X-ray absorption techniques in excited-state studies [13–18]. Ultrafast electron diffraction is another emerging technique able to determine dynamic structural evolution of excited large molecules, especially when used in conjunction with DFT calculations [19].

Twinning experimental excited-state studies with quantum-chemical calculations provides a deep insight into the excited-state character, dynamics and relaxation pathways, well beyond experimental observations. A reasonable agreement between calculated and experimental observables, such as absorption and emission spectra, vibronic structure, or ground- and excited-state vibrational frequencies, is sought to validate the theory. If achieved, it lends credibility to further theoretical conclusions, for example, on electron-density redistribution or structural changes upon excitation. Calculations can identify spectroscopically silent excited states involved in relaxation processes, or reveal excited-state evolution leading to ultrafast photochemical reactions. Computational assessment of electronic coupling within molecular assemblies in ground and excited states is another important task, whose accomplishment would be very important for understanding and development of efficient electron- or energy-transfer systems.

Herein, we discuss the potential, opportunities, challenges and limitations of DFT and TD-DFT in excited-state calculations of d^6 transition metal complexes and organometallics. A brief theoretical introduction compares the merits of several theoretical approaches, outlines the physical basis of TD-DFT and discusses the ways how to describe excited states in a chemically instructive way that could appeal to experimental spectroscopists, photochemists and photophysicists. Following "case-studies" demonstrate applications of TD-DFT to excited states of carbonyl-diimine complexes, Ru^{II} sensitizers or strongly phosphorescent organometallic complexes. It is shown how analysis of TD-DFT results reveals new aspects of low-lying electronic transitions and excited states and their relaxation pathways. A rather delocalized picture of organometallic excited states emerges, while new types of excited states and new relaxation pathways are identified.

2. Theoretical background

Quantum-chemical calculations use either the electronic wavefunction or electron density as the basic variable, leading to *ab initio* and density-functional (DFT) techniques, respectively [20–22]. Semiempirical methods are derived from the wavefunction approach by using various simplifications and replacing some integrals by empirically determined parameters [20].

2.1. Wavefunction-based techniques

This large group of computational techniques uses the Hartree–Fock approximation, whereby each electron is assumed to move in an averaged central field of all other electrons. Solution of HF equations yields energies of molecular orbitals ϕ_i, whose wavefunctions are expressed as linear combinations of atomic orbitals (*i.e.* the basis set) χ_j:

$$\phi_i = \sum_j c_{ij}\chi_j \tag{1}$$

The electronic wavefunction of a given electronic state is constructed from the occupied molecular orbitals as a Slater determinant. HF equations completely neglect electron correlation, which arises from instantaneous interactions between electrons. It affects ground-state properties and is essential for excited-state calculations. Electron correlation is in all wavefunction-based techniques treated by subsequent configuration interaction (CI), whereby the total electronic wavefunction of any electronic state of the system is expanded in terms of Slater determinants which describe singly, doubly, and multiply excited electron configurations [22]:

$$\Psi = C_0\Phi_0 + \sum_{a,k} C_a^k \Phi_a^k + \sum_{ab,kl} C_{ab}^{kl}\Phi_{ab}^{kl} + \sum_{abc,klm} C_{abc}^{klm}\Phi_{abc}^{klm} + \cdots \tag{2}$$

Herein, C are expansion coefficients, Φ_0 the zeroth order ground-state wavefunction (Slater determinant), and the successive terms correspond to singly, doubly, triply, *etc*. excited configurations. The subscripts a, b, c, . . . specify the orbitals occupied in the zeroth order ground-state configuration from which electrons are excited into virtual orbitals k, l, m, ... Depending on the particular technique, the expansion (2) is usually truncated and only singly (CIS), or singly and doubly excited (CISD) configurations are retained. Energies of the ground and excited states are obtained as eigenvalues of the CI expansion, while further excited-state properties can be calculated from the corresponding excited-state wavefunction. Correlation effects being well accounted for, *ab initio* CI techniques are able to calculate also excited-state potential energy surfaces, including regions of state crossing. Wavepacket propagation on such potential energy surfaces then provides an alternative way to calculate electronic absorption, emission and resonance Raman spectra [23–29], or to model ultrafast dynamics and photochemistry [26,27,29–36].

Remarkable results were obtained on mixed-ligand metal carbonyls using multiconfiguration complete active space techniques based on CASSCF, as will be illustrated in Section 4. In CASSCF-type techniques, molecular orbitals are divided into inactive (low-lying, doubly occupied in all states considered), virtual (high-lying, unoccupied in all states considered) and active, which lie energetically between the inactive and virtual sets and are most relevant for the ground and excited states investigated. Only the electrons in the active orbitals are correlated. In other words, HF is used to construct the zeroth order wavefunction and electron correlation is described by an expansion (2) using only those Slater determinants, which can be constructed from the active orbitals and the correlated electrons. Subsequent second-order perturbational MS-CASPT2 or variational multi-reference CI (MRCI) [27,37] calculations are applied to the CASSCF wavefunctions to account for dynamic electron correlation. MRCI generally gives less accurate spectra than MS-CASPT2, but appears to be more reliable for calculations of excited-state potential energy surfaces in the regions where the states interact with each other (avoided crossings) [37]. Generally, the CASPT2 method is chosen if the initial CASSCF wavefunction describes well the static correlation energy and all the electronic states in question. Otherwise, the MRCI approach is preferred since it partly compensates for the errors caused by limiting the active space size [27,37]. Complete active space methods are computationally very demanding. They could not be fully automated and their use requires "computational experimenting". Selection of the active orbitals (*i.e.* the active space) and the number of correlated electrons is a subjective choice of the researcher. The quality of the calculation increases with the active-space size and the number of correlated electrons, but the computational demands increase much faster. At present, these calculations are limited by 16 correlated electrons and 15 active orbitals. The size of the CI expansion and number of reference configurations used in MRCI calculations also affect the quality of the results.

Coupled-cluster (CC) methods present another approach to configurational interaction [22,38]. The electronic wavefunction is expanded in terms of singly, doubly, *etc*. multiply excited determinants through an action of an exponential operator e^C on a zeroth order HF wavefunction. The cluster operator C of

an N-electron system is a sum of operators $C_1 + C_2 + \cdots + C_N$, which create singly, doubly, *etc*. excited configurations. This is, in principle, a size-consistent, accurate technique for calculating electronic energies. It is computationally very demanding and, for practical reasons, only several terms are retained in the expansion. For example, in commonly used CC singles and doubles (CCSD), only operators corresponding to singly and doubly excited configurations are retained. Transition energies are calculated using the equation-of-motion (EOM-CCSD). At the time of writing, applications were limited to small transition metal complexes, $Ni(CO)_4$ [27] and $Cr(CO)_6$ [39]. Coupled-cluster methods are rapidly evolving and applications to larger organometallic systems can be expected.

Semiempirical techniques present relatively simple and computationally undemanding approach to wavefunction-based calculations. INDO and its version developed by Zerner (ZINDO) [20] appear to be the most suitable ones to calculate UV–vis spectra of transition metal complexes [40–47]. Some of the integrals are neglected while others are replaced by parameters, which are optimized by comparison with *ab initio* calculations and experimental spectra. Part of the dynamic correlation energy and solvent effects are thus included in the empirical parameters. Excitation energies are obtained as eigenvalues of a CI expansion using a number of singly excited configurations. Up to 1250 configurations have been used [46]. Each excited state is described by a linear combination of singly excited configurations and the corresponding spectral transitions can be easily visualized as linear combinations of the corresponding one-electron excitations from occupied to virtual orbitals.

2.2. Density functional theory

DFT [22,38,48–55] is conceptually different from the wavefunction-type techniques discussed above. It is based on the Hohenberg–Kohn theorem, which states that the ground-state energy and all other ground-state properties are uniquely determined by the electron density $\rho(\mathbf{r})$, where $\mathbf{r}$ specifies the position in space. Moreover, it follows [48,53] that the true density corresponds to the lowest energy. This allows us to optimize both the energy and density by variational procedures.

DFT is rigorously applicable to the lowest state of given symmetry or spin multiplicity. It can be used to calculate both closed- and open-shell systems. Either restricted or unrestricted Kohn–Sham approach (the latter abbreviated UKS) can be employed for open-shell calculations. Lowest triplet excited states of molecules with close-shell ground states are commonly calculated by UKS.

The electron density $\rho(\mathbf{r})$ equals to a sum over all occupied Kohn–Sham (KS) orbitals $\phi_i(\mathbf{r})$:

$$\rho(\mathbf{r}) = \sum_{i=1} n_i |\phi_i(\mathbf{r})|^2 \tag{3}$$

where n_i is the occupation number of the orbital $\phi_i(\mathbf{r})$. (Note that UKS calculations of open-shell systems express the total electron density $\rho(\mathbf{r})$ as a sum of α and β densities and $\phi_i(\mathbf{r})$ denote the corresponding spin-orbitals.) The Kohn–Sham orbitals $\phi_i(\mathbf{r})$ are expressed by Eq. (1) in terms of atomic orbitals, becoming thus the DFT equivalents of molecular orbitals of wavefunction-based methods. Their physical validity was analyzed in detail by Baerends and co-worker [50], who has proposed that the KS orbitals "may be expected to be more suitable for use in qualitative MO theory than either HF or semiempirical orbitals". In several studies, KS orbitals were found to be very similar in shape to MOs calculated by HF [56], semiempirical [46], or CASSCF/CASPT2 [57,58] techniques. For metal complexes, KS orbitals are usually more delocalized than those obtained by semiempirical [46] and CASSCF/CASPT2 [57,58] calculations. This will be demonstrated in Section 3.3, using $[Ru(Me)(X)(CO)_2(dab)]$ complexes as an example. The total ground-state DFT wavefunction is described by a Slater determinant composed of occupied KS orbitals. Its knowledge is the key to calculations of ground-state properties.

KS orbitals $\phi_i(\mathbf{r})$ and their energies ε_i are obtained by solving Kohn–Sham equations (4):

$$\left\{ -\frac{\hbar^2}{2m_e}\nabla_1^2 - \frac{e^2}{4\pi\varepsilon_0}\sum_{I=1}^{N}\frac{Z_I}{R_{I1}} + \frac{e^2}{4\pi\varepsilon_0}\int \frac{\rho(\mathbf{r}_2)}{r_{12}}\,\mathrm{d}\mathbf{r}_2 + V_{XC}(\mathbf{r}_1) \right\} \times \phi_i(\mathbf{r}_1) = \varepsilon_i\phi_i(\mathbf{r}_1) \tag{4}$$

In addition to the kinetic and coulombic potential energy, KS equations contain the potential V_{XC}, which describes the non-classical electron exchange and correlation. Solving KS equations requires a functional which assigns the energy value to the given electron density. Although an exact and universal functional should, in principle, exist, its exact mathematical expression is unknown because of the exchange-correlation term V_{XC}. Therefore, approximate functionals have to be used. Indeed, recent progress of DFT was marked by a continuing development and improvement [59] of approximations to the exchange-correlation potential V_{XC}, which is defined [22] as a functional derivative of the exchange-correlation energy E_{XC}:

$$V_{XC}[\rho] = \frac{\delta E_{XC}[\rho]}{\delta\rho} \tag{5}$$

The choice of the functional is critical for the success of a DFT calculation, introducing some arbitrariness. The first generation of functionals used the local density approximation (LDA), whereby only the electron density value at a given point in space determines the contribution of this point to the exchange-correlation energy. All non-local effects are neglected. This approximation treats the molecule as containing a homogeneous electron gas in the field of a continuously distributed positive charge. Although this is obviously an unrealistic picture, LDA functionals yield relatively accurate structures. The generalized gradient approximation, GGA, add a term reflecting a gradient of electron density at a given point, accounting in part for an inhomogeneous distribution of electron density and some non-local effects. Functionals based on LDA and GGA only are called pure density functionals. BP86 [60,61] is a typical example used herein. It includes Becke's gradient correction to the local exchange expression in conjunction with Perdew's gradient correction to the local correlation. Recently, shape-corrected pure functionals such as SAOP [62] were developed for spectro-

scopic applications. They perform well for electronic transitions of small molecules and several types of transition metal complexes [63]. As to our experience [64], pure functionals, including SAOP, strongly underestimate energies of CT transitions of low-valent d^6 metal complexes, while much better results are obtained using the so-called hybrid functionals. They are constructed as a mixture of a DFT exchange-correlation, usually approximated by GGA, and a Hartree–Fock exchange, which can be evaluated exactly, using exchange integrals between KS orbitals. Relative contributions of various terms to a functional are somewhat arbitrary parameters that have been determined to achieve the best correspondence with experiments or *ab initio* calculations. For example, the popular B3LYP functional [65] contains three parameters, which specify the contributions of the HF exact exchange, local exchange, gradient-corrected exchange and gradient-corrected correlation [49]. In our studies of carbonyl-diimine complexes, discussed in Section 3, we found the PBE0 functional [66,67] (Eq. (6), also called PBE1PBE) to give the best results. It mixes 25% of HF exchange ($a = 0.25$) with the GGA exchange-correlation [49]:

$$E_{XC}^{PBE} = E_{XC}^{GGA} + a(E_X^{HF} - E_X^{GGA}) \tag{6}$$

Changing the relative contribution of the HF exchange by varying the coefficient a can have dramatic effects on electronic transition energies and shapes of the simulated spectra [58,68].

In summary, DFT is a high-level technique, which accounts for a large part of correlation energy [69] without the necessity of a large CI expansion. It is therefore much faster and computationally less demanding than wavefunction-based *ab initio* methods, which employ the Hartree–Fock approximation and subsequent CI treatment (Eq. (2)). The computer time needed for DFT calculations is less sensitive to the number of atoms and the size of the basis sets, owing to newly developed procedures of linear scaling. This enables high-quality calculations for relatively large molecules. It is also easier to include medium (solvent) effects [48]. Importantly for experimental chemists, results of DFT calculations can be communicated in the familiar terms of molecular orbital theory.

2.3. Time-dependent DFT calculations of electronic transitions

TD-DFT calculations of electronic transitions are based on the response of the ground-state electron density to the oscillating optical field. The use of the ground-state density makes the question of the validity of the Hohenberg–Kohn theorems to excited states irrelevant. Therefore, TD-DFT is, in principle, applicable to all excited states, regardless their spin and symmetry. For a closed-shell molecule, TD-DFT can be used to calculate the whole manifolds of singlet as well as triplet excited states, provided that the transition energies are smaller than the vertical ionization potential. TD-DFT has been successfully applied to open-shell organic radicals [70] and transition metal complexes [63,71,72], as well as triplet excited states [72]. TD-DFT theory and its application to excitation energies of metal carbonyls, α-diimines, sandwich complexes, Werner complexes and metallotetrapyrroles were reviewed recently [63]. It should be stressed that no universal computational procedure exists and different types of chemical systems and electronic transitions may require us to employ different functionals.

To obtain energies and oscillator strengths of electronic transitions, TD-DFT treats a molecule as being subjected to a time-dependent perturbation caused by an oscillating electrical field of the incident light [22,54,63,73–75]. The electron density becomes time-dependent:

$$\rho(\mathbf{r}, t) = \sum_{i=1}^{n} n_i |\phi_i(\mathbf{r}, t)|^2 \tag{7}$$

TD-DFT calculations use the linear response approximation, whereby changes of the electron density are assumed to be proportional to the changes of the external field. Behavior of a molecule in a time-dependent field is described by a set of time-dependent Kohn–Sham equations:

$$\left\{ -\frac{\hbar^2}{2m_e}\nabla_1^2 - \frac{e^2}{4\pi\varepsilon_0}\sum_{I=1}^{N}\frac{Z_I}{R_{I1}} + \frac{e^2}{4\pi\varepsilon_0}\int \frac{\rho(\mathbf{r}_2, t)}{r_{12}}\,\mathrm{d}\mathbf{r}_2 + V_{XC}(\mathbf{r}_1, t) + V_{ext}(t) \right\} \phi_i(\mathbf{r}_1, t) = i\hbar\frac{\partial}{\partial t}\phi_i(\mathbf{r}_1, t) \tag{8}$$

Herein, $V_{ext}(t)$ represents the time-dependent external perturbation, *i.e.* the electromagnetic field of the incident light, which oscillates with a frequency ν. Practical computations use the adiabatic approximation, whereby the exchange-correlation potential $V_{XC}(\mathbf{r}_1, t)$ is assumed to be time-independent, identical to that used in stationary ground-state DFT calculations.

Solution of time-dependent KS equations (8) yields the time-dependent electron density, from which a frequency-dependent dynamic polarizability $\alpha(\nu)$ is obtained. It can be expanded in terms of energies of the electronic transitions (denoted n) and the corresponding oscillator strengths f_n:

$$\alpha(\nu) = \frac{4\pi^2 e^2}{m_e}\sum_n \frac{f_n}{(\nu_n - \nu_0)^2 - \nu^2} = \frac{\hbar^2 e^2}{m_e}\sum_n \frac{f_n}{(E_n - E_0)^2 - E^2} \tag{9}$$

The summation is carried over all electronic excited states. E_0 and E_n are the energies of the ground- and nth electronic excited state, respectively, while ν_0 and ν_n are the corresponding frequencies ($E = h\nu$). The transition energies ($E_n - E_0$) are the "poles", *i.e.* discontinuities, of this function, which occur every time the incident light energy equals the excitation energy: $E = (E_n - E_0)$, or, in other words, the incident light frequency ν equals the transition frequency $\nu_n - \nu_0$. Oscillator strengths are the corresponding residua. The oscillator strength is defined as

$$f_n = \left(\frac{4\pi m_e}{3e^2\hbar}\right)\nu_n|\mu_n|^2 = \left(\frac{2m_e}{3e^2\hbar^2}\right)E_n|\mu_n|^2 \tag{10}$$

where μ_n is the transition dipole moment. The oscillator strength determines the absorption band intensity, that is its integrated

area A: $f_n = 6.257 \times 10^{-19} A$ (for A in $m^2\ mol^{-1}\ s^{-1}$). The intensity of the corresponding electronic transition is given by μ_n. Eq. (10) shows that the actual band intensity (area) depends also on the transition energy. Thus, for a given μ_n value, the absorption band will be more intense if it occurs in the UV or blue part of the spectrum than in the red or NIR.

In Section 3, we use the relation between f_n and absorption band areas to simulate absorption spectra. They are modeled as composed of Gaussian bands of an area A, centered at E_n. A typical value of 0.4 eV, estimated [76] from experiments, is used for the bandwidth (full-width at half-maximum).

As was shown in a recent review [63], TD-DFT can provide transition energies that are accurate within a few tenths of eV. A case study of MnO_4^- has even demonstrated the potential of TD-DFT to calculate vibronic transitions and to deal with difficult problems of avoided crossings, configurational mixing and vibronic coupling between excited states [77]. It was also noted [63] that, for some transitions, the calculated transition energies depend strongly on the metal–ligand distance. This underlines the importance of optimization of the ground state structure. In some studies, different functionals were used to calculate the structure and transitions of the same molecule. It also follows that rigorous comparison with experimental spectra would require to calculate the vibronic structure [70,77] or to identify the 0–0 transition in the experimental spectrum. In practice, however, calculated vertical transition energies are simply compared with the absorption band maxima. TD-DFT calculations may suffer problems from the local nature and wrong asymptotic behavior of approximate functionals, which affect long-range CT and high-lying electronic transitions, respectively. These issues will be discussed in the following two sections.

2.4. Kohn–Sham orbital energies and TD-DFT treatment of charge-transfer states

While energies of occupied orbitals correspond to vertical ionization potentials in both DFT and HF, the meaning of virtual orbitals and their energies differ [50,54,56,78–80]. For an N-electron system, a HF virtual orbital describes an extra electron in a reduced state containing $N+1$ electrons. Energies of HF virtual orbitals thus equal to electron affinities. The situation is different for DFT, where virtual KS orbitals describe an electron in an average field of the remaining $N-1$ electrons. Hence, the KS orbitals are stabilized by an attractive interaction with the positive hole left behind in the manifold of the lower-lying orbitals. Energies of KS virtual orbitals are therefore lower (more negative) than the corresponding electron affinities. Clearly, virtual KS orbitals describe excited electrons and differences between energies of virtual and occupied KS orbitals are good approximations to electronic transition energies. This is a convenient starting point for TD-DFT calculations of electronic transitions, so long as they are localized at a single molecular site. However, a problem arises for charge-transfer excited states where the electron is excited from a donor orbital to an acceptor orbital, which is localized at a different part of the molecule. Because of their inherently local nature, approximate pure DFT functionals (whereas LDA or GGA) do not describe properly the long-range electron–hole separation (r_{eh}). They overestimate the stabilization of the acceptor orbital by the electron–hole attraction since the excited electron is treated as originating in the spatial region of the acceptor site, instead of the distant donor. The acceptor orbital is then calculated at far too low energy. The energy difference between the acceptor and donor orbitals, which contributes importantly to the TD-DFT transition energy, is then too small and the CT transition energies are underestimated, sometimes by as much as 1–2 eV. TD-DFT treatment of CT transitions has been theoretically analyzed in detail by several authors [54,78–81]. It has been shown [54,80] that the error can be traced down to the lack of the "derivative discontinuity" in approximate functionals, whereby the exchange-correlation functional should jump discontinuously when the electron number at a particular site changes.

This problem has been identified for charge-separated states of electron-transfer dyads [79], donor–acceptor complexes [81], small molecules such as peptides [82], weakly interacting systems [83] or MLCT states of carbonyl-diimine complexes, which will be discussed in Section 3. It becomes severe in systems with large spatial separation between the excited electron and hole and/or with weak interaction (overlap) between the donor and acceptor orbitals. TD-DFT calculations thus shift to low energies only the CT excited states with long-range charge separation while other, more localized, states are calculated correctly. This could lead to wrong predictions of excited-state ordering and UV–vis spectral patterns, whereby high-lying CT states are wrongly calculated as the lowest ones. Such a situation arises, for example, in the case of $[Re(t\text{-stpy})(CO)_3(bpy)]^+$, for which TD-DFT (B3LYP, vacuum) incorrectly predicts stpy → bpy LLCT singlet and triplet states to be the lowest excited states [84]. On the other hand, CASSCF/MRCI rejects them to much higher energies, correctly assigns the lowest state as ^{3}IL(stpy), being closely followed by Re → bpy ^{3}MLCT [84], in line with the experimental assignment [85].

Potential energy curves of CT states along the donor–acceptor distance coordinate present another problem for TD-DFT calculations [78,79,81]. Again, this is caused by the local character of DFT functionals, which does not account well for the $-1/r_{eh}$ dependence of the electron–hole interaction. At long distances, where the donor–acceptor orbital overlap is negligible, transition energy to a CT state should equal to $IP + EA - 1/r_{eh}$, where IP and EA are the ionization potential and electron affinity, respectively. Instead, TD-DFT leads to a simple KS orbital energy difference $-\varepsilon_{donor} + \varepsilon_{acceptor}$. Since $\varepsilon_{acceptor}$ is lower than EA, the asymptotic energy is too low, and a wrong flat or even repulsive shape of the potential energy curve results [79].

Notwithstanding these theoretical problems, charge-transfer excited states of transition-metal complexes can be calculated by TD-DFT with a good precision, as will be shown in the remaining sections of this review. Errors caused by the local nature of pure DFT calculations can be diminished by using hybrid functionals, which introduce a fractional contribution of the non-local HF exchange. The asymptotic function of CT states is then improved by the term $-a/r_{eh}$, while the HF exchange also increases the energy of the acceptor orbital. We have found

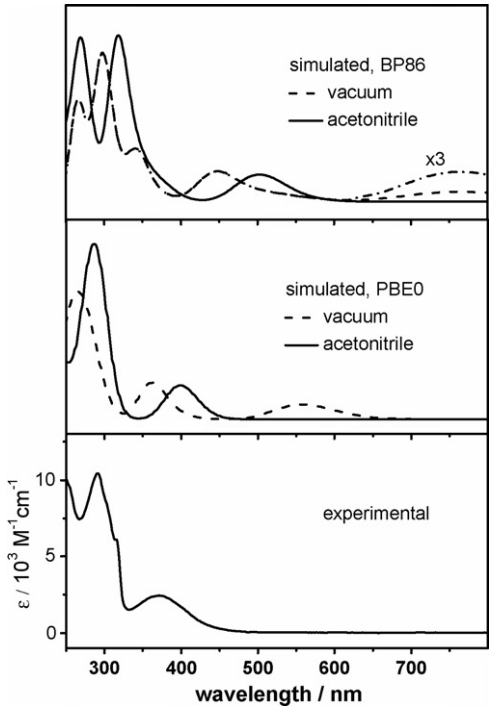

Fig. 1. Effect of the functional and solvent on TD-DFT simulation of the UV–vis spectrum of [Re(Cl)(CO)$_3$(bpy)]. Full line: spectra calculated in CH_3CN. Dashed line: spectra calculated in vacuum. Top: pure functional BP86. Middle: hybrid functional PBE0. Bottom: experimental spectrum measured in CH_3CN. Simulations performed with Gaussian 03. CH_3CN solvent modeled by CPCM.

(Section 3.1, Fig. 1) that energies of MLCT and related CT states in carbonyl-diimine complexes are still underestimated by hybrid functionals B3LYP or PBE0, but much less than by pure DFT functionals, such as BP86. As to our experience, PBE0 ($a = 0.25$) gives better results than B3LYP. The superior performance of PBE0 for CT transition was noted before for organic molecules, small metal complexes as well as Ru-bpy sensitizers [49,86–88]. Energies of some CT transitions can be increased closer to experimental values by increasing the HF fraction a in a hybrid functional [58]. However, this is an arbitrary procedure, which can hardly be recommended. Recently, a special functional called CAM-B3LYP was developed [89] to deal specifically with long-range CT transitions. It is a hybrid functional in which the fraction of the HF exact exchange varies in different regions of a molecule. Its good performance was demonstrated for CT transitions in a zincbacteriochlorine–bacteriochlorine complex, for which other DFT approaches failed [79].

TD-DFT treatment of charge-transfer transitions can be much improved by including the solvent into the calculation, using continuous models COSMO or CPCM [90], which are discussed in Section 2.8. Solvent effects on TD-DFT calculated CT transitions are further demonstrated in Section 3.1, Fig. 1, and Section 3.3 using *fac*-[Re(Cl)(CO)$_3$(bpy)] and [Ru(Me)(X)(CO)$_2$(dab)] as examples, respectively. The TD-DFT/hybrid functional/CPCM approach works well even for intermolecular electron transfer, as was demonstrated by a precise calculation of ion-pair CT energies of $[Pt(NH_3)_4]^{2+}[W(CN)_8]^{3-}$ in water [91]. It is well possible that a large part of the errors in some previous TD-DFT calculations originated in neglecting the solvent. This can be related to the tendency of vacuum DFT calculations to exaggerate the orbital mixing in some kinds of polar metal–ligand bonds and overestimate charge separation upon excitation. These effects are largely suppressed by the electrostatic field of the solvent.

2.5. Long-range behavior of DFT functionals and TD-DFT calculations of high-lying states

Most of the currently used functionals do not describe correctly the electron–nucleus attraction at large distances from an atom or a molecule, which should decrease as $-1/R$ [49]. Pure DFT functionals decrease exponentially, that is too fast, underestimating the electron–nucleus interaction at large distances. This incorrect asymptotic behavior affects energies and shapes of higher virtual orbitals. It diminishes the reliability of DFT calculations of those properties which depend on high-lying virtual orbitals, such as electronic transitions to higher or Rydberg excited states, charge separation, electrical polarizabilities or electron affinities, and calculations of excited states of extended π systems [54,82]. This problem is amended by hybrid functionals, for which the electron–nucleus coulombic energy decreases as $-a/R$. The PBE0 hybrid functional shows a good performance even for high-lying states [87,92]. As an alternative, asymptotically correct pure-DFT functionals are being developed, for example SAOP [62] or HCTH(AC) [49,82]. Indeed, TD-DFT calculations of high-lying states improve enormously when these corrected functionals are used [62,82]. Other approaches use different functionals for short and long-range interactions, respectively. A new, promising, procedure combines DFT, using a GGA functional, with wavefunction CC techniques to describe short- and long-range interactions in the same chemical system, respectively [93].

2.6. Calculations of relaxed excited-states

Characterization of relaxed excited states and interpretation of their TRIR and emission spectra require the knowledge of the equilibrium geometry of the investigated state in given medium. Whereas the ground state optimization is a standard task treated by any quantum-chemical program, excited-state optimization is a more complex problem. Since DFT is rigorously valid only for the lowest state of given spin and symmetry, it is possible to optimize the structure of the lowest-lying triplet state by a separate DFT calculation. This is usually done using unrestricted KS calculations (UKS), where Kohn–Sham equations are solved separately for α and β spins. The lowest triplet state is described by an open-shell single-determinant wavefunction and its energy relative to the ground state can be calculated as a difference between the total UKS triplet energy and the total ground-state DFT energy. This approach to calculate excited-state energies is sometimes called ΔSCF. (Note that before the advent of TD-DFT, the ΔSCF technique was used to calculate vertical excitation energies and optimize structures of higher states, even if DFT is not rigorously applicable to such cases. See Refs. [75,63] for further discussion.)

Alternatively, excited-state structures can be optimized by calculating TD-DFT excitation energy as a function of the normal coordinates q_i. Its analytical gradients $\delta E/\delta q_i$ are known and their effective implementation [94] makes it possible to calculate excited-state structures of relatively large transition metal complexes. Contrary to UKS, the TD-DFT approach is applicable to any excited state. This technique is not (yet) completely straightforward and several problems can be encountered. In principle, all interacting states should be taken into account, which makes optimization time demanding. Close-lying states can cross during optimization, which could cause the calculation to diverge or oscillate. In such cases, it is necessary to limit the calculation to the lowest triplet and use the UKS approach, as discussed above. As far as lowest triplet states are concerned, it still remains to be shown whether the UKS or the TD-DFT technique is superior. As an example, TD-DFT optimization of two close-lying triplet excited states and UKS calculation of the lowest triplet of [Re(NCS)(CO)$_3$(bpy)] are demonstrated in Section 3.2.

Calculations of TD-DFT energies as a function of specific coordinates can be used to interpret photochemical reactivity. This procedure was successfully used to calculate photochemical CO dissociation from carbonyl-hemes by calculating TD-DFT excitation energies and excited-state characters as a function of a Fe–CO distance [95,96]. In another study, photochemistry of [Cr(CO)$_5$(PH$_3$)] and [Fe(CO)$_4$(PH$_3$)] was modeled [97] by wavepacket propagation on excited-state potential energy surfaces calculated by TD-DFT.

Vibrational frequencies of an excited state are calculated [98] using second derivatives of its UKS total energy or the TD-DFT excitation energy. Vibrational frequencies and normal coordinates are obtained as eigenvalues and eigenvectors of the Hessian matrix, whose elements $\delta^2 E/\delta q_i \delta q_j$ define vibrational force constants. Absolute values of calculated frequencies depend on the quality of the basis set and method used. Therefore, quantitative comparison with experimental values often requires linear scaling of calculated wavenumbers. For example, a scaling factor of 0.961 was recommended [99] for calculations with B3LYP and a double-ζ basis set.

The amount of the HF exchange in the functional strongly affects the structural displacement of an excited state relative to the ground state [70] and, hence, the gradient of the excited-state potential energy surface in the region of vertical excitation. This is, in turn, important for calculations of vibronic structure, resonant enhancements of Raman bands and photochemical reactivity.

2.7. Representations of electronic transitions and excited states

In addition to transition energies, oscillator strengths and symmetries, which are directly provided by TD-DFT calculations, we need a physical insight into characters of electronic transitions and excited states. Their qualitative nature is described by the changes in electron-density distribution relative to the ground state. This leads to the familiar categories such as LF, MLCT, LLCT, *etc*. In general, an excited state can be characterized by the molecular orbitals involved in the transition, plots of changes of electron density upon excitation or by changes of electron population (or charges) at individual atoms or molecular fragments. TD-DFT can be, in principle, used for any excited state, while UKS (ΔSCF) calculations are limited to the lowest triplet state. As to our experience, TD-DFT and UKS often give slightly different characters of the lowest triplet. This is demonstrated in Fig. 2 (right) and Fig. 3 (left) for the a^3A'' lowest triplet of [Re(Cl)(CO)$_3$(bpy)], for which TD-DFT predicts somewhat larger contribution from an IL $\pi\pi^*$ excitation than UKS.

TD-DFT describes excited states as linear combinations of Slater determinants corresponding to singly excited configurations. Each of these determinants is constructed from ground-state KS orbitals, by replacing one KS spin-orbital, which is occupied in the ground-state, with a virtual one. This approach allows us to represent each electronic transition T by a linear combination of one-electron excitations between pairs of ground-state KS orbitals ϕ_i, ϕ_j:

$$\sum_{i<j} c_{ij\mathrm{T}}(\phi_i \rightarrow \phi_j) \tag{11}$$

The square of the expansion coefficient $c^2_{ij\mathrm{T}}$ specifies the contribution of the one-electron excitation from the orbital ϕ_i to the virtual orbital ϕ_j, expressed as a fraction of 1 or in %, provided that the coefficients are normalized to 1 or 100, respectively: $\sum_{i,j} c^2_{ij\mathrm{T}} = 1$ (or 100).

Such orbital representation allows us to visualize electronic transitions by comparing the shapes of the initial and final optical orbitals ϕ_i and ϕ_j. (See Fig. 8 for a particular example.) This procedure is straightforward only if the investigated transition is satisfactorily described by a single one-electron excitation. (Note, that for a single predominant ($c^2_{ij\mathrm{T}} > 0.9$) excitation, the "hole" and the excited electron are mostly localized in the orbitals ϕ_i and ϕ_j, respectively.) However, it often happens that the electronic transition affects many electrons in a molecule and the corresponding expansion (11) contains many one-electron excitations with similar weight, blurring the orbital picture. To overcome this problem, it is possible to perform a unitary transformation of the whole set of the occupied and virtual KS orbitals to construct "natural transition orbitals", ϕ'_i, ϕ'_j [100,101]. This new set of orbitals is equivalent to the original KS set, but describes each electronic transition as a single one-electron $\phi'_i \rightarrow \phi'_j$ excitation, with the corresponding coefficient $c^2_{ij\mathrm{T}}$ larger than about 96%.

The orbital representation is especially instructive when based on TD-DFT, since the KS orbitals describing the ground and excited state are the same. This is not true for UKS, which describes the lowest triplet state by KS spin-orbitals that are generally different from the ground-state KS orbitals. (This orbital relaxation in UKS actually accounts for multiple excitations, which TD-DFT treats by the expansion (11).) On the other hand, an UKS-calculated lowest triplet state can be described by its lower- and higher-lying singly occupied orbitals, see Fig. 14 for an example.

Another very instructive way of describing excited states uses difference electron densities, calculated by subtracting the excited- and ground-state electron densities. This representa-

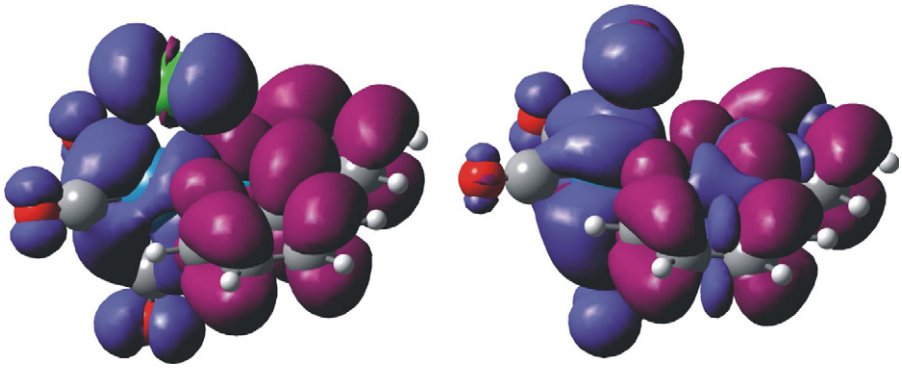

Fig. 2. Electron-density redistribution in the b^1A' (left) and a^3A'' (right) states of [Re(Cl)(CO)$_3$(bpy)] in CH_3CN. TD-DFT (PBE0, CPCM) calculation. Left: electron-density redistribution upon the lowest allowed $a^1A' \rightarrow b^1A'$ transition. Right: electron-density difference between the lowest triplet state a^3A'' and the ground state calculated by TD-DFT at optimized triplet geometry. Blue and violet colors show the regions of decreased and increased electron density, respectively. The Cl atom faces up.

tion shows the regions of increased and decreased electron population. Resulting plots of the difference density are very instructive for CT states, where these regions are separated. The difference density picture becomes less clear if the excitation is highly localized in the same region of space, due to constructive and destructive additions. (For difference density description of excited states of various metal complexes, see Figs. 2, 3, 6, 9, 11, 12 and 15. Comparison of Figs. 8 and 9 demonstrates the merits of orbital and difference density representations.)

An interesting representation has been proposed [54,102], which defines electron detachment and attachment densities and plots them separately. They represent the regions depopulated and populated upon excitation, respectively, but do not simply correspond to the negative and positive difference-densities. Detachment and attachment densities have been nicely used to visualize the reactive excited state at various stages of CO dissociation from carbonylhemes [95,96].

Lowest triplet states are sometimes characterized by plots of the spin density calculated by UKS. Although depicting the regions of the molecule that are affected by excitation, spin densities seem to be less pictorial than electron-density differences, since the populated and depopulated regions cannot be distinguished. This is visualized in Fig. 3, which compares the difference density and spin density of the lowest triplet state of [Re(Cl)(CO)$_3$(bpy)]. Similar comparison is made in Figs. 14 and 15 for a cyclometallated Ir complex. Moreover, spin-polarization of low-lying doubly occupied orbitals contributes to the spin density but not to the density difference (note the blue regions in Fig. 3, right).

As another way to describe excited states, population analysis can be used to calculate changes of electron density on individual molecular fragments. The Mulliken or atoms in molecule (AIM) approaches can be used to divide the electron density or charges among molecular fragments or atoms. The AIM technique was, for example, used in conjunction with DFT to calculate the charges on the metal and the ligands in the complexes [M(bpy)$_2$(L)$_2$] (M = Ru, Os; L = NCS, CN) and to assess the effects of polar solvents on the intramolecular charge distribution [88]. Mulliken population analysis was used in our work on carbonyl-diimine complexes (Section 3.3), as well as other excited-state studies [57,103,104].

Natural transition orbitals, shapes of populated and depopulated MOs, electron-density differences and attachment/detachment densities represent rigorously only vertical transitions, which occur without any change in the molecular structure. These representations are thus most amenable to depict optically populated Franck–Condon states. When applied to relaxed excited states, they actually compare the excited- and ground-state electronic structures at the excited-state

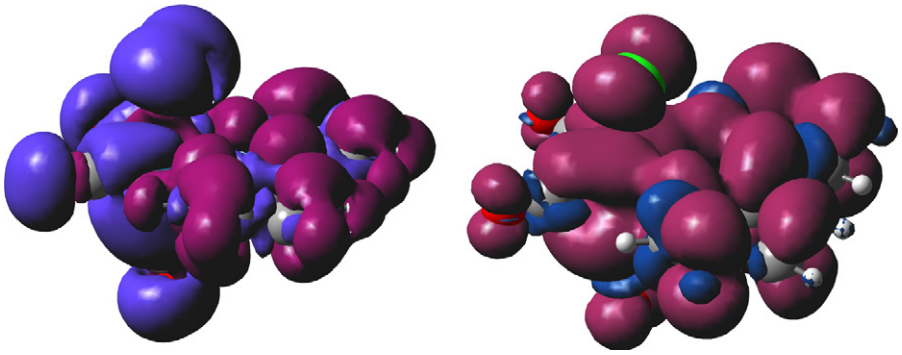

Fig. 3. Two representations of the a^3A'' lowest triplet state of [Re(Cl)(CO)$_3$(bpy)] in CH_3CN. UKS (PBE0, CPCM) calculation. Left: electron-density difference between the lowest triplet state a^3A'' and the ground state calculated at optimized triplet geometry. Blue and violet colors show the regions of decreased and increased electron density, respectively. Right: spin density in the a^3A'' state, expressed as a difference between α and β spin densities. The Cl atom faces up.

Table 1
DFT calculated one-electron energies and compositions of selected highest occupied and lowest unoccupied molecular orbitals of [Re(Cl)(CO)$_3$(bpy)] expressed in terms of composing fragments

	MO	E (eV)	Prevailing character	Re	CO	Cl	bpy
BP86 vacuum	LUMO (a′)	−3.66	π^* bpy	3	4	1	92
	HOMO (a″)	−5.07	Cl + Re	33	19	46	2
	HOMO − 1 (a′)	−5.16	Cl + Re	28	16	52	4
	HOMO − 2 (a′)	−5.79	Re + CO	64	33	1	2
PBE0 vacuum	LUMO (a′)	−2.78	π^* bpy	3	2	1	94
	HOMO (a″)	−5.97	Re + Cl + CO	43	21	34	2
	HOMO − 1 (a′)	−5.97	Re + Cl + CO	40	18	38	4
	HOMO − 2 (a′)	−6.67	Re + CO	68	30	0	2
PBE0 CPCM (MeCN)	LUMO (a′)	−2.42	π^* bpy	3	3	1	93
	HOMO (a″)	−6.47	Re + CO + Cl	53	25	18	4
	HOMO − 1 (a′)	−6.55	Re + CO + Cl	51	24	20	5
	HOMO − 2 (a′)	−6.97	Re + CO	67	31	0	2

equilibrium geometry, which can be quite different from that of the ground state. The same is true for descriptions of excited states during photochemical reactions. On the other hand, singly-occupied excited-state orbitals, population analysis of molecular fragments, or triplet spin densities can be used to describe excited states at any chosen geometry.

2.8. Calculation of molecules in condensed media

Carbonyl-diimine complexes are often strongly solvatochromic, whereby their visible and near-UV absorption bands shift to higher energies as the polarity of the solvent increases [105–113]. The magnitude of this shift is qualitatively related to the extent of metal–ligand charge separation upon the corresponding electronic transition. It is often used as an experimental diagnostic criterion for MLCT spectral bands [106]. This solvatochromism is caused by large changes in the molecular dipole moment upon MLCT transitions. Usually, the ground state is more polar than the excited state, being more strongly stabilized in polar solvents. Similar effects are seen for emission from ^{3}MLCT states, which depends even more strongly on the rigidity of the medium (rigidochromism) [105]. These medium effects put in question the ability of quantum-chemical calculations on isolated molecules in vacuum to describe electronic transitions and excited states in a condensed phase.

In our calculations (Section 3), we have used continuum solvent models CPCM or COSMO, as incorporated in the software packages Gaussian 03 and Turbomole, respectively. In brief, the solvent medium is treated as a dielectric continuum, characterized by its dielectric constant [48,90]. The solute molecule is placed in a solvent cavity, which follows the shape of the solute. Interaction between the solute's electrons and the electrostatic field exerted by solvent charges at the boundary of the cavity is included into the calculation in the same way as electron–nuclei interactions.

Results discussed in Sections 3 and 6 show that a reasonable agreement between TD-DFT and experimental MLCT transition energies can only be obtained if the solvent is included. (See Fig. 1 for a representative example.) The same is true for structural optimization and calculations of vibrational and emission spectra of relaxed excited states. Solvent also affects the composition and energies of high-lying molecular orbitals, which often become more localized relatively to those calculated in vacuum. This is documented for [Re(Cl)(CO)$_3$(bpy)] in Table 1. For [Re(NCS)(CO)$_3$(bpy)], we have observed (Section 3.2, Ref. [111]) that the continuum models work better for more polar CH_3CN than toluene or CH_2Cl_2. However, a linear correlation has been found between calculated (B3LYP/CPCM) and experimental CT transition energies of $[Ru(bpy)_2(CNx)Cl]^+$ (CNx = 2,6-dimethylphenylisocyanide) in a series of solvents with polarity ranging from benzene to water [114]. On the other hand, only small solvent effects were calculated for symmetrical metal carbonyls $V(CO)_6^-$, $Cr(CO)_6$ and $Mn(CO)_6^+$, in accordance with their negligible experimental solvatochromism [115]. Solvent effects seem to be most important for calculations of polarizable, mixed-ligand complexes, and transitions which affect the periphery the molecule.

More sophisticated models based on the Poisson–Boltzmann equation [48,90] can deal with complicated situations of non-homogeneous environments where the solvent–solute interface is composed of regions of different dielectric properties, such as proteins. Other techniques to treat the environment would employ combinations of quantum and molecular mechanics (QM/MM). In the case of specific solvent–solute interactions, it is necessary to explicitly include solvent molecules within the first solvation sphere and to use a continuum solvent model for such a supersystem. This procedure has been applied to the solvent-dependent "light-switch" $[Ru(phen)_2(dppz)]^{2+}$ [101], see Section 7.

Finally, it should be noted that static environment models may not be sufficient for full understanding of the behavior of charge-transfer excited states. For example, charge localization in MLCT-excited $[Ru(bpy)_3]^{2+}$ seems to be driven by solvent fluctuations. Environment dynamics can also be important in excited-state relaxation, as well as in energy- or electron-transfer processes. Hybrid methods combining quantum-chemical calculations with molecular dynamics (MD) should be able to model and explain dynamic effects of both intramolecular and environment fluctuations on spectra and excited-state behavior.

3. Case studies: excited states, photophysics and photochemistry of carbonyl-diimine complexes

Carbonyl-diimine complexes of d^6 metals, namely Re^I, Ru^{II}, Cr^0, W^0 are noted for their diverse photoactivity [106,107,116]. For example, $[M(CO)_4(N^\wedge N)]$ (M = Cr, W; N^N = α-diimine, polypyridine) and $[Ru(X)_2(CO)_2(N^\wedge N)]$ undergo ultrafast CO ligand substitution from ^{1}MLCT states [106,116–121]. Rhenium complexes $[Re(L)(CO)_3(N^\wedge N)]^{n+}$ show an exceptionally broad range of photobehavior, which can be tuned by variations in L and N^N, or by the medium [107,122–124]. Depending on the actual situation, their near-UV irradiation populates long-lived strongly emissive excited states, triggers ultrafast electron- or energy transfer, ligand isomerization, or homolysis of the Re–L bond. Robustness, synthetic flexibility, and the excited-state sensitivity to external stimuli make these complexes exceptionally promising active units of supramolecular assemblies, sensors, probes, sensitizers or phosphorescent dyes for OLEDs. Their excited states can be conveniently studied by TRIR since the ν(C≡O) IR bands are very sensitive reporters of electron-density changes at the Re atom.

In this section, we will discuss computational studies on several Re^I and Ru^{II} carbonyl-diimine complexes to demonstrate the great potential of DFT and TD-DFT for understanding their spectra, excited states, photochemistry and photophysics. These cases are elaborated in a tutorial way, emphasizing effects of the computational procedure, especially the functional and continuous solvent models. Calculations were performed with Gaussian 98, Gaussian 03 or TURBOMOLE software.

3.1. Electronic transitions and excited states of fac-[Re(Cl)(CO)$_3$(bpy)]: effects of computational procedures

Earlier experimental studies [125–129] have assigned the lowest allowed electronic transitions and the emissive lowest triplet state of this complex as Re → bpy MLCT, possibly with an admixture from Cl → bpy LLCT [113]. This assignment was confirmed by our TD-DFT study [130]. The choice of the basis set has only a small effect on the composition of calculated molecular orbitals and transition energies. The calculated vibrational frequencies are more sensitive to the quality of the basis set: the mean error diminishes with enlarging the basis set, of course at the expense of increasing computer time. A reasonable compromise between accuracy and computing costs is the use of double-ζ basis with polarizations functions (6–31g* [131] or cc-pvdz [132]) for light atoms and Stuttgart quasirelativistic effective core pseudopotentials and corresponding optimized set of basis functions for the Re atom [133].

The calculated and experimental UV–vis spectra are compared in Fig. 1. As seen in the top and middle panes, the use of the pure functional BP86 and neglect of the solvent strongly underestimate energies of low-lying electronic transitions. Due to the low oscillator strength of the lowest band, one can erroneously assign the feature calculated by PBE0 in vacuum at ∼370 nm as the lowest allowed transition. This has indeed happened in a previous study [134]. Changing the functional from BP86 to PBE0 shifts the low-lying CT transitions to higher energies by almost 1 eV. Including the solvent amounts to another *ca.* 1 eV shift, regardless of the functional. A very good agreement with the experimental spectrum (Fig. 1) was thus obtained when the hybrid PBE0 functional was used together with the CPCM correction for the CH_3CN solvent. Intense UV transitions, with a prevalent IL $\pi\pi^*$(bpy) character, are much less sensitive to the solvent and functional. The magnitude of the solvent effect is comparable for both functionals.

The errors in BP86 and vacuum calculations of the CT transitions can be understood in terms of KS orbital energies and compositions summarized in Table 1. Changing the functional from BP86 to PBE0, and including the solvent have parallel effects on high-lying occupied MOs, namely decreasing the mixing between the 5dπ(Re) and 3pπ(Cl) orbitals. This is manifested by a decrease and increase of the Cl and Re participation, respectively, in the HOMO and HOMO − 1. The CO participation is about the same for BP86 and PBE0, but increases in the solvent. The HOMO–LUMO energy gap increases from 1.41 to 3.19 eV on changing the functional from BP86 to PBE0 and to 4.05 eV upon including the solvent. The character of the lowest allowed CT transition depends on the functional and solvent accordingly: the pure BP86 functional gives much larger decrease of the electron density on the Cl ligand than PBE0, exaggerating the Cl → bpy LLCT character. For PBE0, the LLCT contribution is larger in vacuum than CH_3CN. It follows that errors in calculating the CT transition energies arise from the erroneous treatment of the long-distance charge transfer from Cl to bpy by DFT. Exaggeration of LLCT contributions [57,58] and underestimation of LLCT energies [84] seem to be common features of TD-DFT calculations with pure functional and/or in vacuum, see also Section 3.3. The [Re(Cl)(CO)$_3$(bpy)] example shows that this error can be minimized by including the HF exchange in the functional and calculating the chromophore in a solvent reaction field [130].

The lowest absorption band of [Re(Cl)(CO)$_3$(bpy)] originates predominantly in the $a^1A' \rightarrow b^1A'$ (96% HOMO − 1 → LUMO) transition. Fig. 2 (left) shows that the electron density is transferred from the whole Re(Cl)(CO)$_3$ fragment to bpy. Such a transition can be seen as mixed Re → bpy MLCT and Cl → bpy LLCT (also sometimes called XLCT), in agreement with an earlier experimental suggestion [113]. However, a delocalized MLLCT (metal–ligand-to-ligand CT) description seems more appropriate. (See the final paragraph of Section 3.2 for further discussion.)

The structure and IR spectra of the lowest triplet excited state were calculated using two approaches: TD-DFT (PBE0, COSMO for CH_3CN) and UKS (PBE0, CPCM for CH_3CN). Both these procedures agree on its A″ symmetry and the Re,Cl(CO) → bpy MLLCT character. However, there are important quantitative differences: TD-DFT predicts smaller depopulation of CO ligands and larger contribution from a $\pi\pi^*$ excitation of the bpy ligand, compare Fig. 2 (right) and Fig. 3 (left). Another way of visualizing the excited-state character is seen in Fig. 3 (right). Herein, the UKS spin density calculated for the lowest ^{3}A″ state indicates regions influenced by excitation. The spin density qualitatively corresponds to the electron-density

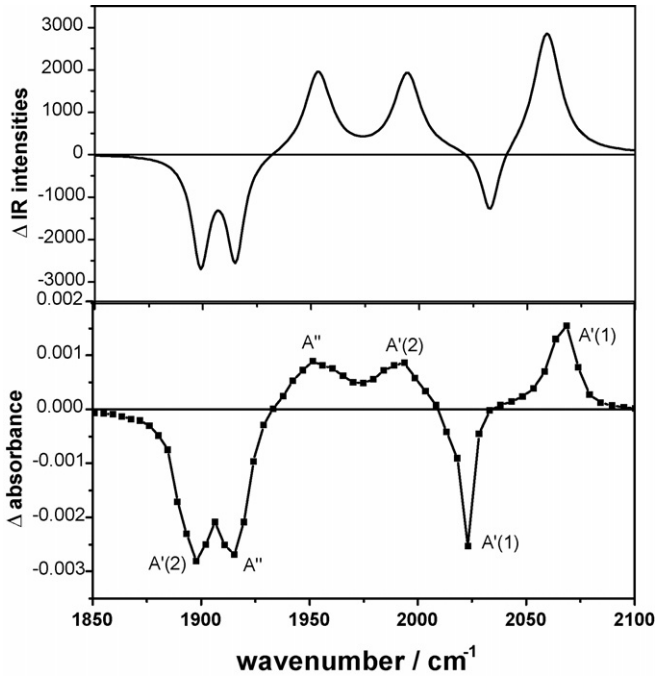

Fig. 4. Comparison of the calculated (top) and experimental (bottom) difference TRIR spectra of [Re(Cl)(CO)$_3$(bpy)] in CH_3CN. The experimental difference spectrum was measured at 2 ns after excitation. Calculated spectrum was obtained as a subtraction of the simulated ground state spectrum from the simulated spectrum of the a^3A'' state. Positive and negative peaks correspond to vibrations of the excited and the ground state, respectively. Calculation: DFT (PBE0/CPCM), Gaussian 03. Triplet state was optimized by UKS. Calculated frequencies are scaled by the factor of 0.963. Gaussian shapes (FWHM = 10 and 15 cm^{-1} for ground and excited states, respectively) were used for the IR bands. Experimental/calculated values (cm^{-1}): 1898/1899, 1915/1915, 2023/2033 (GS); 1952/1953, 1993/1995, 2067/2059 (a^3A'' ES). Assigned according to Ref. [11].

redistribution shown on the left but the populated and depopulated regions cannot be distinguished and some important details, such as the $\pi\pi^*$ contribution, cannot be discerned.

To assess the quality of the DFT models of the lowest triplet, we compare the experimental and calculated (PBE0/CPCM) emission energies and IR spectra in CH_3CN. Both the TD-DFT (2.03 eV, corrected for the difference in zero-point energy, ZPE) and UKS emission energies (2.08 eV, ZPE-corrected) agree well with the experimental value of 2.03 eV [127]. Experimental excited-state IR spectrum (Fig. 4, bottom) shows an upward shift of all ν(CO) bands upon excitation, which is diagnostic of a MLCT character of the excited state [135–138]. The excited-state IR spectrum of the lowest a^3A'' state calculated by UKS matches the experimental one better (Fig. 4, top) than that obtained [111] with TD-DFT, which exaggerates the $\pi\pi^*$(bpy) contribution. (Compare Figs. 2 (right) and 3 (left) for TD-DFT and UKS a^3A'' characters.) BP86 or PBE0/vacuum calculations gave unrealistically low emission energies and only poor match between calculated and experimental IR spectra.

This example clearly demonstrates that the use of a hybrid functional and incorporation of the solvent are essential for modeling CT transitions and triplet states of this type of complexes. A delocalized view of the lowest CT transition and excited state of [Re(Cl)(CO)$_3$(bpy)] emerges, whereby the electron density is excited from the whole Re(Cl)(CO)$_3$ moiety to the bpy acceptor ligand.

3.2. Mixing of MLCT and LLCT characters in low-lying electronic transitions and excited states: the case of fac-[Re(NCS)(CO)$_3$(bpy)]

In the previous section, it was demonstrated that the lowest CT excitation of [Re(Cl)(CO)$_3$(bpy)] originates in mixed dπ(Re)–pπ(Cl) orbitals, amounting to a MLCT–LLCT character mixing or, in other words, to a MLLCT transition. This effect was proposed earlier from spectroscopic studies [107,112,113,139–141] of [Re(Cl)(CO)$_3$(α-diimine)] and [Ru(X)(E)(CO)$_2$(α-diimine)] complexes. Generally, the amount of the LLCT admixture (also known as XLCT) is assumed to increase in the order X = Cl < Br < I. This mixing is difficult to study experimentally since monoatomic halide ligands have no characteristic spectroscopic signatures such as vibrations or NMR signals. Therefore, we have synthesized the complexes [Re(NCS)(CO)$_3$(N^N)] (N^N = bpy, iPr-dab) and studied their UV–vis, resonance Raman, as well as ground- and excited-state IR spectra [111]. The electron-rich, π-donating axial ligand NCS^- is expected to behave similarly to the halides, while changes in the NC stretching frequency would allow us to monitor its electronic depopulation upon excitation.

TD-DFT calculation (PBE0/CPCM) have well reproduced the absorption spectrum of [Re(NCS)(CO)$_3$(bpy)] measured in CH_3CN [111]. The lowest allowed absorption band, which occurs at 3.31 eV, was calculated at 2.93 eV. The agreement between the experimental and calculated spectra is worse in CH_2Cl_2 and toluene, where the lowest absorption band energy is underestimated by 0.78 and 1.0 eV, respectively. It seems that the CPCM model works better for more polar solvents. The lowest allowed transition of [Re(NCS)(CO)$_3$(bpy)] originates 99% in HOMO − 1 → LUMO excitation, the HOMO − 1 being composed of 28% dπ(Re) and 57% pπ(NCS) contributions. LUMO is predominantly (85%) a bpy π^* orbital. Obviously, this transition involves depopulation of both metal and NCS moieties, in line with the expected mixed MLCT–LLCT character (*i.e.* MLLCT). Experimentally, this character mixing was documented [111] by the observation of resonance enhancements of Raman bands due to both the ν(CO) and ν(NC) vibrations, which show that both the Re(CO)$_3$ unit and the NC bond of the NCS^- ligand are affected by the lowest-allowed electronic transition.

The lowest triplet state of [Re(NCS)(CO)$_3$(bpy)] is emissive and relatively long-lived; 23 ns in fluid acetonitrile solution [111]. It was characterized by TRIR spectra, which show that the ν(CO) and ν(NC) bands shift to higher and lower wavenumbers upon excitation, respectively, see Fig. 5. In particular, the higher ν(CO) band, A′(1) shifts by +26 cm^{-1} and the ν(NC) A′ band shifts by −32 cm^{-1} on going from the ground state to the lowest triplet state. Qualitatively, this behavior is fully in line with the proposed mixed MLCT–LLCT character: The upward shifts of ν(CO) vibrations reflect [135–137] the Re → bpy MLCT contribution, whereby the Re → CO π back donation is weakened and the OC → Re σ donation strengthened upon depopulation of dπ(Re) orbitals. At the same time, the downshift of the ν(NC)

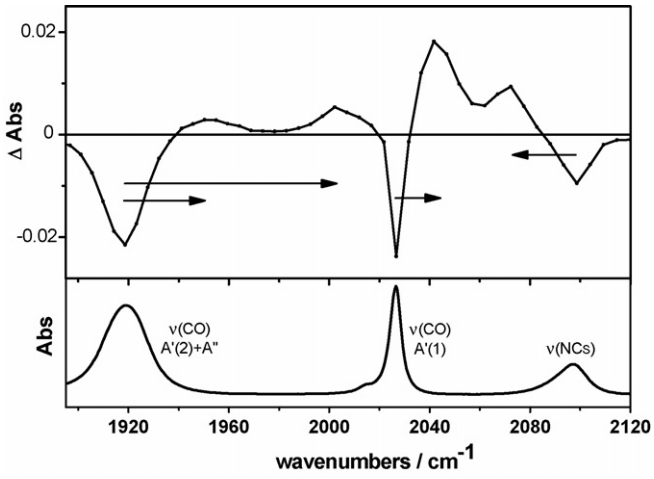

Fig. 5. Top: difference TRIR spectrum of [Re(NCS)(CO)$_3$(bpy)] measured at 1000 ps after 400 nm excitation in CH_3CN. The arrows show band shifts upon excitation. Bottom: ground-state FT-IR spectrum of [Re(NCS)(CO)$_3$(bpy)].

vibration is caused by depopulation of the π bonding N = C = S orbital due to the NCS → bpy LLCT contribution.

TD-DFT calculations have revealed the presence of two close-lying triplet states ^{3}aA′ and ^{3}aA″ occurring at 2.86 and 2.75 eV, respectively. These triplet energies are too close to allow us to decide which state is the lowest one at the actual experimental conditions. Calculated emission energies (2.22 and 2.05 eV, respectively) agree well with the experimental emission band maximum at 2.06 eV, while the existence of two close-lying states is experimentally supported by the observation of a biexponential emission decay in a 77 K glass: 1.3 and 2.7 μs. Despite their similar energies, it was possible to optimize the structures of both triplet states by TD-DFT, calculate the electron-density differences from the ground state and their IR spectra. The electron-density differences clearly show the shift of electron density from the dπ(Re) and π(NCS) to the bpy ligand, *i.e.* the MLCT/LLCT mixing, in both states. The a^{3}A″ state of [Re(NCS)(CO)$_3$(bpy)] (Fig. 6, right) is analogous to the lowest triplet calculated for [Re(Cl)(CO)$_3$(bpy)] (Fig. 2, right). It contains a small ππ*(bpy) admixture, which is absent for the a^{3}A′ state (Fig. 6, left).

UKS calculation (PBE0/CPCM) agrees with TD-DFT on the a^{3}A″ assignment of the lowest triplet. A good correspondence with the experimental excited-state IR wavenumbers was obtained for the a^{3}A″ state calculated by UKS and for the a^{3}A′ state calculated by TD-DFT. Because of the good match between the calculated and experimental IR wavenumbers, we have originally assigned the lowest triplet of [Re(NCS)(CO)$_3$(bpy)] as a^{3}A′, although TD-DFT predicted an unusual order of ν(CO) vibrations [111]. However, the new excited-state 2D IR study [142] seems to agree better with the vibrational assignment calculated by UKS for the a^{3}A″ state. Although this work is still in progress, we may preliminarily conclude that UKS describes the lowest triplet state of [Re(NCS)(CO)$_3$(bpy)] better than TD-DFT.

The qualitative explanation of the ν(CO) and ν(NC) IR shifts proposed above agrees with the calculated depopulation of dπ(Re), π*(CO) and π(NCS) orbitals in both the a^{3}A″ and a^{3}A′ states, see Fig. 6. However, the calculated normal coordinates reveal a more complicated picture, whereby the CO and NCS vibrations, which are uncoupled in the electronic ground state, become strongly mixed upon excitation to either triplet state [111,142]. This vibrational coupling could be the consequence of enhanced electronic coupling between the ligands, which is demonstrated by depopulation of commonly shared Re dπ orbitals, see Fig. 6. Time-resolved 2D IR experiments are in progress to demonstrate this excited-state vibrational coupling experimentally and test the ability of various DFT-based approaches to calculate vibrational normal coordinates [142].

Finally, it is necessary to comment on the excited-state character in [Re(NCS)(CO)$_3$(bpy)], [Re(Cl)(CO)$_3$(bpy)] and related complexes. The use of the LLCT and MLCT labels and talking about mixed LLCT/MLCT electronic transitions and excited states is tributary to the classical, rather localized, view of charge-transfer transitions. From the above discussion, it follows that the lowest electronic transitions and excited states of these complexes can be viewed as delocalized, the electron density being excited from the π system of the entire Re(NCS)(CO)$_3$ moiety to the π* system of the electron-accepting α-diimine ligand. Such transition occur in other types of complexes, such as the famous photosensitizer [Ru(4,4′-(COOH)$_2$-bpy)$_2$(NCS)$_2$]$^{2+}$

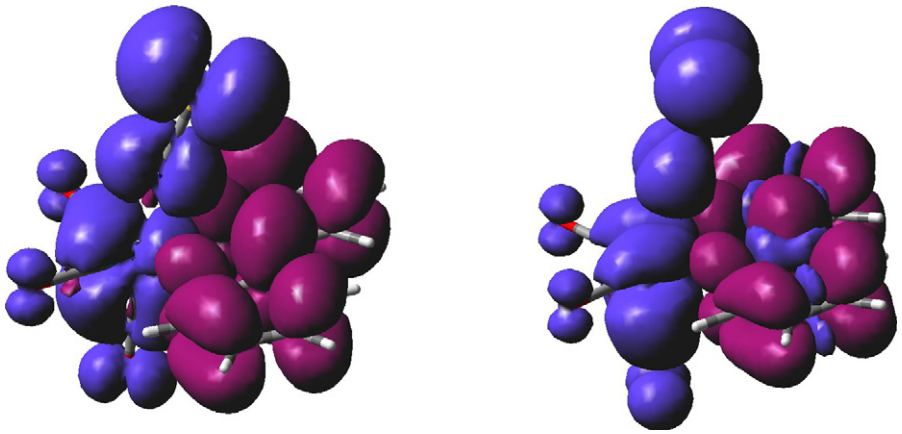

Fig. 6. Change of electron density distribution upon the a^{1}A′ → a^{3}A′ (left) and a^{1}A′ → a^{3}A″ (right) electronic transitions of [Re(NCS)(CO)$_3$(bpy)]. Blue and violet colors show regions of decreased and increased electron density, respectively. Calculated by TD-DFT (PBE0/CPCM) in a CH_3CN solution.

Table 2
The solvent dependence of the two lowest allowed electronic transitions of [Ru(Me)(Cl)(CO)$_2$(Me-dab)]

Transition	PBE0 vacuum	PBE0/CPCM cyclohexane	PBE0/CPCM CH_3CN	Experiment[a]
MLLCT $a^1A' \rightarrow b^1A'$	2.19 (0.013)	2.52 (0.029)	2.90 (0.042)	2.70[b], 2.98[c]
SBLCT $a^1A' \rightarrow c^1A'$	3.07 (0.018)	3.27 (0.029)	3.55 (0.026)	∼3.48[b]

Transition energies (in eV) calculated by TD-DFT (PBE0), solvents modeled by CPCM. Oscillator strengths are in parenthesis.
[a] Experimental data are for [Ru(Me)(Cl)(CO)$_2$(iPr-dab)].
[b] In cyclohexane [57].
[c] In CH_3CN [112].

(Section 6) and phosphorescent Ir^{III} complexes which combine cyclometallated and bpy-type ligands (Section 5). In these cases, the MLLCT notation was introduced, which stands for metal–ligand-to-ligand CT. Obviously, the MLCT and LLCT characters are two limiting cases of MLLCT, whose relative contributions vary with the chromophore structure, the medium and, in theoretical studies, also with the DFT functional.

3.3. Effects of halide ligands: TD-DFT and CASSCF/CASPT2 calculations of [Ru(E)(E′)(CO)$_2$(N,N′-di-Me-1,4-diazabutadiene)] complexes (E = E′ = SnH_3 or Cl; E = SnH_3 or Cl, E′ = CH_3)

Above, we have discussed the mixing between MLCT and halide → diimine LLCT characters in low-lying electronic transitions and excited states in Re complexes. It was shown that TD-DFT tends to underestimate energies of such transitions, unless the calculation includes the solvent. To elucidate this effect further, comparative TD-DFT and CASSCF/CASPT2 studies were performed on the above complexes, with an emphasis on [Ru(Me)(Cl)(CO)$_2$(Me-dab)] [57,58]. TD-DFT(B3LYP/vacuum) and CASSCF/CASPT2 (vacuum) calculations agree very well with each other on the transition energies and characters for complexes which do not contain a halide ligand; that is [Ru(SnH_3)$_2$(CO)$_2$(Me-dab)] and [Ru(Me)(SnH_3)(CO)$_2$(Me-dab)]. Their lowest intense transitions are assigned as $\sigma_2 \rightarrow \pi^*$(dab), the σ_2 orbital being essentially non-bonding with respect to the axial E–Ru–E′ linkage. (Such transitions are called in the literature sigma-bond-to-ligand CT (SBLCT), or $\sigma\pi^*$ [107,123,124,143].) It is followed in energy by Ru → dab MLCT transitions in the near-UV, while the far-UV absorption is dominated by Ru → CO MLCT bands. Transition energies depend only little on the functional. The extent of charge transfer from the E–Ru–E′ moiety (namely the ligands E and E′) to dab upon the lowest transition, calculated as differences in Mulliken populations, is larger for TD-DFT than CASSCF/CASPT2. Spectra calculated by either method agree well with the experimental spectra of [Ru($SnPh_3$)$_2$(CO)$_2$(iPr-dab)] and [Ru(Me)($SnPh_3$)(CO)$_2$(iPr-dab)] in tetrahydrofuran. KS and CASSCF/CASPT2 high-lying occupied orbitals have similar shapes, the KS σ_2 being slightly more delocalized. The situation changes profoundly when a halide ligand is introduced, that is for the complexes [Ru(Cl)$_2$(CO)$_2$(Me-dab)], [Ru(Me)(Cl)(CO)$_2$(Me-dab)] and [Ru(Me)(I)(CO)$_2$(Me-dab)] [57,58]. While CASSCF/CASPT2 (vacuum) still reproduces well the experimental solution spectra, transitions calculated by TD-DFT (B3LYP/vacuum) are underestimated by as much as 0.85 eV. Moreover, TD-DFT transition energies are strongly dependent on the functional, in particular on the amount of the HF exchange [58]. For [Ru(Me)(Cl)(CO)$_2$(Me-dab)], the energy of the lowest allowed transition can be shifted over the whole visible spectral region, from about 1.5 to 4 eV, by increasing the amount of the HF exchange in a BLYP-type functional from 0 to 80% [58]. Moreover, CASSCF/CASPT2 and TD-DFT (both in vacuum) differ in the description of the lowest allowed transition, predicting a predominant MLCT and LLCT contribution, respectively, to the Ru,Cl → dab MLLCT transition [57,58]. TD-DFT consistently predicts *ca*. 1.4 times larger increase of electron density on the dab ligand than CASSCF/CASPT2, regardless the functional. While CASSCF/CASPT2 calculates the high-lying occupied orbitals as mostly Cl-localized 3pπ, followed in energy by 4dπ(Ru) HOMO and HOMO − 1, the corresponding KS orbitals are highly mixed bonding and antibonding 3pπ(Cl)/4dπ(Ru) combinations. The calculated amount of charge transferred upon excitation from the halide ligand increases 1.2–1.3 times on going from the chloride complex to the iodide, regardless the computational method used.

The quality of the TD-DFT calculation of [Ru(Me)(Cl)-(CO)$_2$(Me-dab)] greatly improves upon including the solvent, achieving excellent match with the experimental spectrum, see Table 2. It should be noted that even the non-polar cyclohexane has a remarkably large effect on the calculated transition energy. Improvement of the calculated transition energies on going to the solvent is accompanied by changes in the calculated character of the lowest transition from predominantly Cl → dab LLCT in vacuum to mixed MLLCT in CH_3CN. This is clearly demonstrated by the changes in Mulliken populations summarized in Table 3. Interestingly, the solvent affects mostly the relative

Table 3
Changes in TD-DFT (PBE0) calculated Mulliken populations upon the lowest allowed $a^1A' \rightarrow b^1A'$ transition of [Ru(Me)(Cl)(CO)$_2$(Me-DAB)] in vacuum and CH_3CN

Medium	Ru	Me	X	$(CO)_2$	Me-DAB	Character of the transition
Vacuum	−0.190	−0.006	−0.587	−0.005	0.789	LLCT/MLCT
CH_3CN/CPCM	−0.407	−0.030	−0.317	−0.024	0.779	MLCT/LLCT

depopulation of the Ru and Cl centers while the increase of the electron density on the dab ligand is about the same as in vacuum (∼0.8 e$^-$), larger than that predicted by CASPT2 (0.56 e$^-$). The increase of the TD-DFT transition energy and change in the character on going to the solvent can be traced to the increase of the LUMO–(HOMO − 1) energy gap by 0.73 eV, increase of the 4dπ(Ru) contribution to the HOMO − 1 from 30 to 51% and decrease of the 3pπ(Cl) contribution from 52 to 35%. As for the Re complexes discussed in Sections 3.1 and 3.2, it can be concluded that the TD-DFT calculations in vacuum overemphasize the long-range Cl → dab CT (see Section 2.4). This is largely corrected by placing the molecule into the electrostatic field of the solvent cavity.

3.4. Identification of a "dark" state involved in excited-state relaxation: the case of fac-[Re(Cl)(CO)$_3$(5-NO$_2$-phen)]

Introduction of a nitro group on a polypyridine ligand changes profoundly the photophysical and photochemical properties of their complexes with d^6 metals. Namely, they become non-emissive and the excited-state lifetimes shorten by several orders of magnitude [129,144–148]. To understand this effect, we have studied the model complex [Re(Cl)(CO)$_3$(5-NO$_2$-phen)] by TRIR spectroscopy and TD-DFT calculations [149]. UV–vis spectra calculated by TD-DFT (PBE0/CPCM) in CH$_3$CN almost exactly reproduce the experimental spectrum, see Fig. 7.

The lowest absorption band encompasses two allowed transitions: S_2 (99% HOMO − 1 → LUMO) and S_4 (97% HOMO − 1 → LUMO + 1), which are represented in Fig. 8 by the orbitals involved. It follows that both these transitions have a Re(Cl)(CO)$_3$ → 5-NO$_2$-phen MLLCT character, S_2 being much more delocalized over the NO$_2$ group than S_4. TRIR spectra measured immediately after excitation [149] show upshifted ν(CO) bands typical for a triplet MLLCT state. The large shift value (+69 cm^{-1} for the A′(1) band) indicates an extensive charge separation due to delocalization of the excited electron onto the nitro group. This state is converted with a 10 ps time constant into another excited state, which then decays to the ground state with a 30 ps time constant. The intermediate state is characterized by IR bands that occur at slightly lower wavenumbers than the corresponding ground-state bands (−11 cm^{-1} for the A′(1) band). Such downward shifts usually signify a ππ* ^{3}IL character of the excited state responsible [136]. TD-DFT calculation performed at the ground-state geometry has identified four close-lying triplets that occur in a narrow energy range 2.49–2.87 eV. Figs. 8 and 9 show one-electron excitations and electron-density differences, respectively, for the first three triplets. It follows that T_1 and T_2 are ^{3}MLLCT states, in which the excited electron density is partly delocalized over the NO$_2$ group. T_1 contains an admixture from a ππ* IL excitation, similar to that seen for the a^{3}A″ states of [Re(L)(CO)$_3$(bpy)] (L = Cl, NCS), see Sections 3.1 and 3.2. The T_3 state is an intraligand ^{3}nπ* state, which involves transfer of electron density from the non-bonding orbitals localized on the O atoms of the NO$_2$ group to the π* system of the 5-NO$_2$-phen ligand, see Fig. 9, right. The close energetic proximity of the three lowest triplets T_1, T_2 and T_3 prevented us from optimizing their structures, calculating IR spectra and deciding their energetic order after relaxation. In fact, any of these states can become the lowest relaxed triplet. Nevertheless, TD-DFT calculations still allow us to understand the unusually fast deactivation of excited states of nitro-polypyridyl complexes: Optical excitation of ^{1}MLLCT state(s) is followed by an ultrafast intersystem crossing to a ^{3}MLLCT state, documented by the upshifted IR spectrum seen immediately after excitation. T_2 is the most likely candidate, because of its large charge separation. It is converted in 10 ps to a lower-lying triplet state that shows a typical ^{3}IL TRIR spectrum. It can be identified with the calculated ^{3}nπ* IL state (T_3), which involves excitation of the NO$_2$ group. This state then decays to the ground state in 30 ps. It follows that nitration of the phen ligand introduces a ^{3}nπ* IL state between the ^{3}MLLCT state and the ground state, providing a fast pathway for efficient decay to the ground state [149].

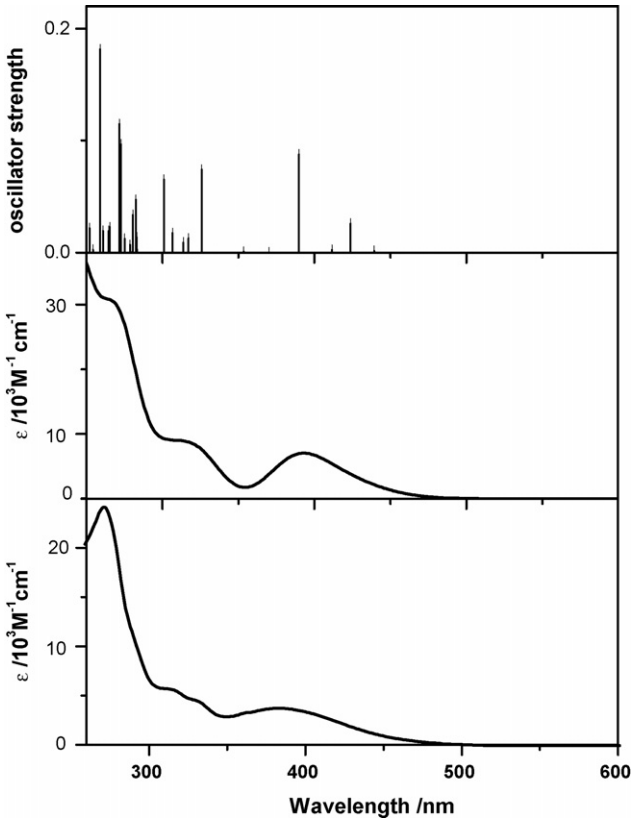

Fig. 7. Electronic transitions calculated for *fac*-[Re(Cl)(CO)$_3$(5-NO$_2$-phen)] in CH$_3$CN (top), simulated absorption spectrum (middle) and experimental absorption spectrum measured in CH$_3$CN (bottom). From Ref. [149].

This case demonstrates that TD-DFT calculations can indicate the presence of low-lying states, which are not apparent in optical spectra (absorption or emission) but play an important role in excited-state deactivation. It also shows that it is difficult to optimize excited-state structures and identify the energetic order of *relaxed* excited states, if they lie too close in energy and have the same symmetry (no symmetry in this case). As far as representations of electronic transitions are concerned (Section 2.7), it should be noted that maps of electron density differences

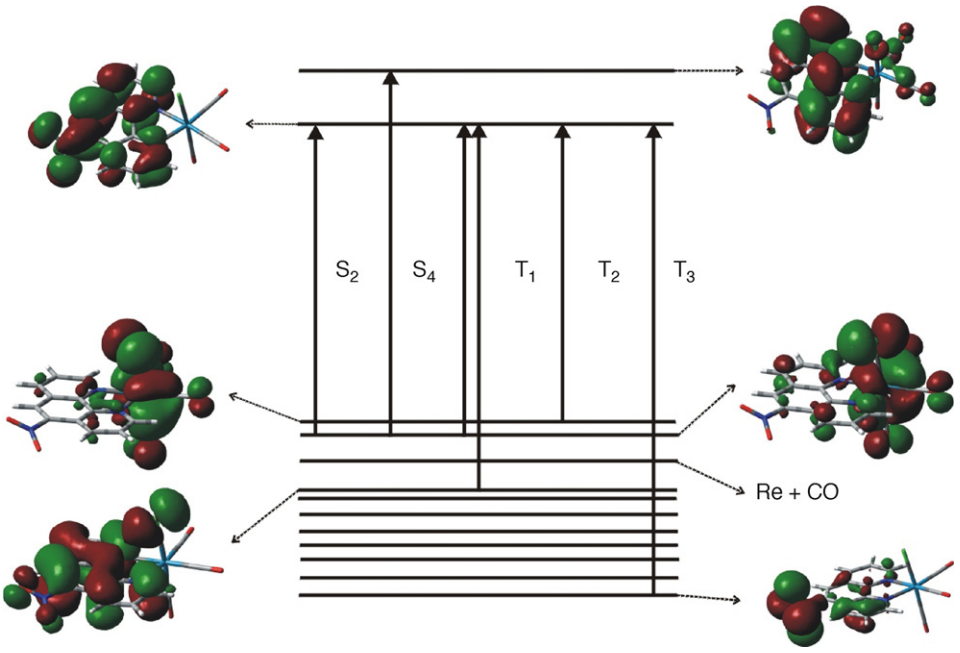

Fig. 8. Qualitative scheme of frontier molecular orbitals of *fac*-[Re(Cl)(CO)$_3$(5-NO$_2$-phen)] calculated by DFT (PBE0/CPCM for CH$_3$CN). The arrows show principal one-electron excitations contributing to the specified low-lying electronic transitions. (Two contributing excitations are shown for T$_1$.) The Cl atom lies above the Re(5-NO$_2$-phen) plane. From Ref. [149].

are more informative than the one-electron orbital representation, compare Figs. 8 and 9.

3.5. Photochemistry of trans(X, X)-[Ru(X)$_2$(CO)$_2$(bpy)]

The complexes *trans*(*X*, *X*)-[Ru(X)$_2$(CO)$_2$(4,4′-R$_2$-bpy)] (X = Cl, Br, I, R = H, C(O)OPr^i, C(O)OH or Me) undergo photochemical CO substitution by a solvent molecule, which is accompanied by shift of a halide ligand X from the axial to the equatorial position, see Eq. (12) [120,121,150–152]

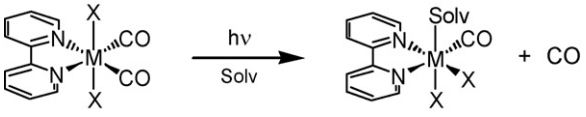

(12)

Quantum yields are rather high but decrease on changing the halide ligand from Cl to Br and I: a near-unity value was reported [150] for [Ru(Cl)$_2$(CO)$_2$(bpy)], while values of 0.68 and 0.34 were determined [121] for [Ru(Br)$_2$(CO)$_2$(4,4′-(COOH)$_2$-bpy)] and [Ru(I)$_2$(CO)$_2$(4,4′-(COOH)$_2$-bpy)], respectively.

An ultrafast TRIR study [117] of the photochemistry of *trans*(*X*, *X*)-[Ru(X)$_2$(CO)$_2$(bpy)] (X = Cl, I) has revealed that optical excitation (400 nm) results in a femtosecond CO dissociation, see Scheme 1. For both complexes, the CO dissociation first produces a monocarbonyl intermediate. Its was identified by comparing the experimental ν(CO) frequency with those calculated by DFT for various possible CO-loss products: It is a *trans*(*X*, *X*)-[Ru(X)$_2$(CO)(bpy)] species with the X–Ru–X bond slightly bent toward the vacant position [117]. This intermediate then undergoes a shift of one halide ligand to the vacant equatorial position and solvent coordination. This reaction occurs with a time constant 13–15 ps for the chloride and 55 ps for the iodide. For X = Cl, this is the only photochemical process, which takes place with a 100% efficiency. The situation is different for X = I, where the CO dissociation competes with intersystem crossing to an unreactive triplet state, which is characterized by broad,

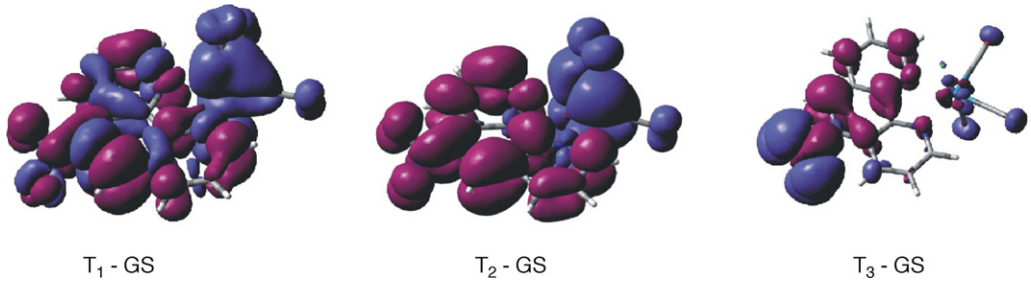

Fig. 9. Changes of electron density distribution between the T$_1$, T$_2$, and T$_3$ excited states and the ground state of *fac*-[Re(Cl)(CO)$_3$(5-NO$_2$-phen)]. Blue and violet colors show regions of decreased and increased electron density, respectively. Calculated by TD-DFT (PBE0, CPCM for CH$_3$CN, ground-state geometry). From Ref. [149].

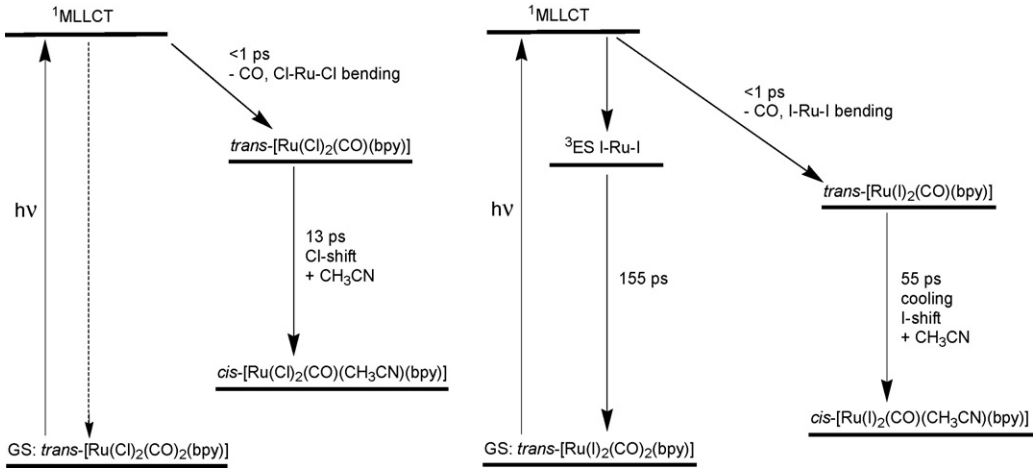

Scheme 1. Mechanism of photochemical CO substitution/isomerization of *trans*(X, X)-[Ru(X)$_2$(CO)$_2$(bpy)]. Left: X = Cl, right: X = I.

slightly downshifted IR feature. This state decays to the ground state with a 155 ps lifetime, see Scheme 1, right.

TD-DFT calculations [117] have shown that, for both complexes, the lowest singlet excited state is a^1B_2 Ru,X → bpy ^{1}MLLCT. It is closely followed in energy by the b^1A_1 Ru,X → bpy ^{1}MLLCT state, which is populated by a spectroscopically allowed transition. The electron density in both these states is transferred from the π orbitals of the XRuX unit to the π* system of the bpy ligand. Intuitively, it is not clear why such ^{1}MLLCT excitation should result in an ultrafast CO dissociation, which obviously occurs directly from the optically excited (Franck–Condon) states on a femtosecond timescale. Apparently, the ^{1}MLLCT states acquire a dissociative character through an avoided crossing with higher-lying LF-type state(s) along the reaction coordinate. The same behavior is exhibited by ^{1}MLCT excited states of [Cr(CO)$_4$(bpy)] and some other mixed-ligand metal carbonyls [27,29,31,97,153–157]. The different behavior of chloro and iodo complexes can be explained by comparing their excited-state diagrams, Fig. 10, which show a remarkable difference between the triplet manifolds of the two complexes.

The two lowest lying triplet states a^3A_1 and a^3B_2 of [Ru(Cl)$_2$(CO)$_2$(bpy)] have a ^{3}MLLCT character. They are well separated in energy from all other triplet states. On the other hand, [Ru(I)$_2$(CO)$_2$(bpy)] possesses four triplet states in a very narrow energy range 2.23–2.36 eV. Two of these states, a^3A_2 and a^3B_1, correspond to reorganization of electron density around the I–Ru–I axis, Fig. 11. The ν(CO) IR bands of the a^3A_2 state were calculated by TD-DFT (in vacuum) to be downshifted from their ground state positions. Comparison with the experimental TRIR spectrum thus indicates that the unreactive state(s), populated in parallel to the CO dissociation, are indeed the IRuI-localized triplets, which are denoted ^{3}ES in Scheme 1.

It was suggested [117] that the presence of low-lying IRuI-localized triplets a^3A_2 and a^3B_1 is responsible for the photoreactivity of [Ru(I)$_2$(CO)$_2$(bpy)] being different from the chloro complex. Intersystem crossing from the reactive ^{1}MLLCT states b^1A_1 and, possibly, a^1B_2 to IRuI-localized triplets a^3A_2 and a^3B_1 is very fast because of larger spin-orbit coupling (due to I and Ru atoms) and different symmetries of the ^{1}MLLCT states and the IRuI-localized triplets. It is competitive with the CO dissociation. The photochemical quantum yield is then determined

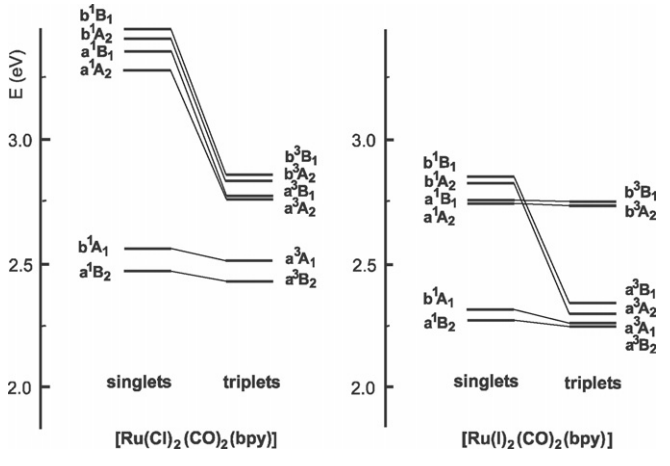

Fig. 10. Singlet and triplet excited-state manifolds of *trans*(Cl, Cl)-[Ru(Cl)$_2$-(CO)$_2$(bpy)] (left) and *trans*(I, I)-[Ru(I)$_2$(CO)$_2$(bpy)] (right). The connecting lines relate singlet and triplet states of a comparable orbital origin. Calculated by TD-DFT (PBE0, COSMO for CH_3CN, ground-state geometry). Note that UKS calculates IRuI-localized a^3A_2 to be the lowest triplet state of the iodo complex. From Ref. [117].

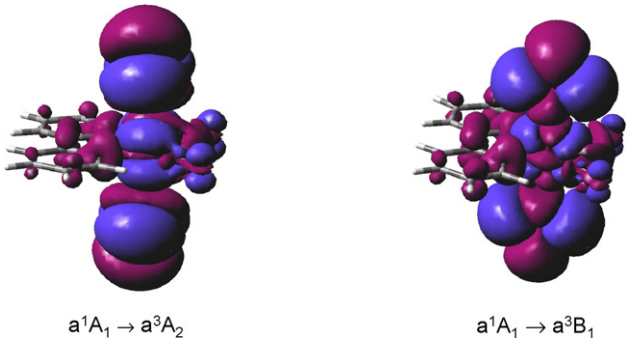

Fig. 11. Changes of electron density distribution upon the $a^1A_1 \rightarrow a^3A_2$ and $a^1A_1 \rightarrow a^3B_1$ triplet electronic transitions of *trans*(I, I)-[Ru(I)$_2$(CO)$_2$(bpy)]. Blue and violet colors show regions of decreased and increased electron density, respectively. Calculation: TD-DFT (PBE0, CPCM for CH_3CN, ground-state geometry).

by branching between the reaction and intersystem crossing. For the chloro-complex, the analogous Cl–Ru–Cl states are energetically not accessible. Intersystem crossing to ^{3}MLLCT states a^3A_1 and a^3B_2 is slower, because of the same symmetry and lower spin-orbit coupling.

This case again demonstrates the ability of TD-DFT to reveal photochemical mechanisms and identify states which are silent in electronic spectroscopy but influence the photophysical and photochemical behavior.

4. Spectra and photochemistry of metal carbonyls: the question of M → CO MLCT *versus* LF excited states

Traditionally, UV–vis spectra and photochemistry of transition metal carbonyl complexes have been interpreted in terms of low-lying, weak LF transitions, arising from excitation between π bonding and σ antibonding metal d-orbitals, and intense M → CO MLCT transitions (further denoted MLCT(CO)) at higher energies [158–160]. Photochemical ligand dissociation was believed to occur from the lowest LF states, usually triplets. This view has changed in 1996 by a CASSCF/CASPT2 study [161] of $Cr(CO)_6$ and $Ni(CO)_4$ which identified the lowest-lying transitions as orbitally forbidden MLCT(CO), instead of LF. Following DFT [156] and TD-DFT [115,162] studies have further confirmed this assignment, the latter with a much better quantitative agreement with the experiment. It was realized that a low-lying set of CO-based acceptor orbitals results from interaction between π^* orbitals on individual CO ligands. The ultrafast [163] CO photochemical dissociation is now attributed to Franck–Condon ^{1}MLCT(CO) excited states. Calculation of potential energy curves have shown that ^{1}MLCT(CO) states become dissociative through avoided crossings with higher-lying ^{1}LF states, which occur along the M–CO reaction coordinate [153,156,157,164].

The effect of the metal on MLCT(CO) and LF states in isoelectronic complexes $V(CO)_6^-$, $Cr(CO)_6$, and $Mn(CO)_6^+$ was investigated by TD-DFT both in vacuum and a solvent using various functionals [115]. Energies of LF states were calculated to decrease slightly on going from V to Cr and Mn, while the MLCT(CO) energies increase in the same order. The LF state was found to be the lowest and spectrally observable only in $Mn(CO)_6^+$. For both $V(CO)_6^-$ and $Cr(CO)_6$, it lies at higher energies than MLCT(CO) [115]. Although the effects of the functional and solvent are relatively small, it was found that the hybrid B3LYP functional and COSMO treatment of the CH_3CN solvent give a better match with the experiment than pure functionals and/or vacuum calculations [115].

MLCT(CO) states are the lowest excited states also in mixed-ligand carbonyl complexes, where the hetero-ligand is not an electron acceptor. In a combined theoretical and spectroscopic study of [W(CO)$_4$(en)] [103], we have found that TD-DFT quite accurately calculates the energy of the lowest allowed transition (B3LYP, vacuum: 2.35 eV; PBE0/CH_3CN: 2.89; Expt.: 2.71 eV) and assigns it as 97% HOMO → LUMO ^{1}MLCT(CO), in contrast with the previous empirical [165] ^{1}LF assignment. Calculated electron-density redistribution (Fig. 12, left) actually reveals that this transition has a more complex character, involving transfer of electron density from the equatorial $W(CO)_2$ unit to the axial CO ligands [103].

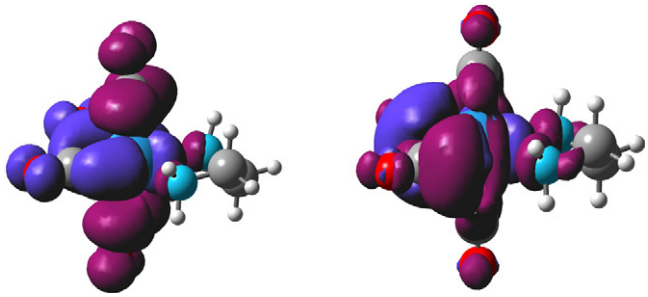

Fig. 12. Change of electron density distribution upon the $a^1A \rightarrow a^1B$ (left) and $a^1A \rightarrow a^3B$ (right) electronic transition of [W(CO)$_4$(en)]. Note the difference between the singlet and triplet states, which can be seen as $W(CO_{eq})_2 \rightarrow CO_{ax}$ MLLCT and predominantly $W \rightarrow CO_{eq}$ MLCT, respectively. Calculations: $a^1A \rightarrow a^1B$, left: TD-DFT, B3LYP, CPCM for CH_3CN, ground-state geometry. $a^1A \rightarrow a^3B$ (right): UKS, B3LYP, CPCM for CH_3CN, a^3B optimized geometry. Blue and violet colors show regions of decreased and increased electron density, respectively.

TRIR spectroscopy allowed us to measure the IR spectrum of the relaxed ^{3}MLCT(CO) state in CH_3CN and determine its lifetime; ∼156 ps [103]. Unlike the corresponding singlet, this state is unreactive, decaying to the ground state. The ν(CO) vibrations are shifted downwards relative to ground state values, as can be expected for excitation of electron density into π^*(CO) orbitals. This assignment of the excited-state IR spectrum is supported by a good match with a DFT-calculated (UKS, CH_3CN) IR spectrum of the lowest triplet state a^3B [103,166]. Calculated emission energy also supports the assignment of the emission seen in low-temperature glasses to the a^3B state. UKS optimization of the a^3B state revealed extensive structural differences from the ground-state: opening of the C_{eq}–W–C_{eq} angle by 20°, closing of the N–W–N bite angle by 5°, and bending of the equatorial W–C–O units by 8°. Finally, UKS-calculated redistribution of electron density (Fig. 12, right) shows that the a^3B state can be described as almost pure ^{3}MLCT(CO) state, arising from electron excitation from the 5dπ(W) orbital into the π^* orbitals of the equatorial and, to a lesser extent, axial CO ligands. The largest increase in electron population is seen on the carbon atoms of the equatorial CO ligands, Fig. 12 (right).

MLCT(CO) states were also identified computationally as the lowest states in pentacarbonyl complexes [$Cr(CO)_5(PH_3)$] [97] and [W(CO)$_5$(piperidine)] [64]. They elude experimental characterization in solution because of ultrafast photochemical dissociation of the heteroligand. Nevertheless, emission [167] and TRIR [168] spectra measured for [W(CO)$_5$(piperidine)] in low-temperature glasses were later reassigned [64] by TDDFT to a ^{3}MLCT(CO) state. The prompt photochemical loss of the heteroligand was rationalized by potential energy curves calculated by TD-DFT (pure functionals, vacuum) [97] for [$Cr(CO)_5(PH_3)$]. They show that avoided crossings with higher-lying ^{1}LF states render low-lying ^{1}MLCT(CO) states dissociative along the Cr–PH_3 coordinate, whereas energy barriers arise along Cr–CO coordinates.

[W(CO)$_5$(4-NC-pyridine)] represents another interesting case [64,167,169] The lowest absorption band is highly sol-

vatochromic and attributed to a W → 4-NC-pyridine MLCT transition. It is closely followed in energy by a weaker near-UV band, whose maximum position does not much depend on the solvent. Traditionally, it was assigned as a LF band. Photochemistry and photophysics of this and related complexes [153,158,167,169] was interpreted by a thermal equilibrium between the unreactive ^{3}MLCT(4-NC-pyridine) and a dissociative ^{3}LF states. TD-DFT (B3LYP, vacuum) has well reproduced the UV–vis spectrum in non-polar methylcyclohexane, confirming the lowest band as MLCT(4-NC-pyridine) and reassigning the near-UV band as MLCT(CO) [64]. The MLCT(CO) transition involves transfer of electron density from the W atom and, less, the axial CO to the four equatorial CO ligands. The lowest triplet state of [W(CO)$_5$(4-NC-pyridine)] was characterized by TRIR and TR^3 spectra as ^{3}MLCT(4-NC-pyridine). It shows typical upward shifts of ν(CO) vibrations, while the ν(C≡N) vibration of 4-NC-pyridine shifts downwards by ∼130 cm^{-1}, due to reduction of the 4-NC-pyridine ligand upon excitation. Vibrational frequencies calculated for the lowest triplet state agree well with the experimental values and allowed us to assign the bands seen in TRIR and TR^3 spectra [64]. TD-DFT also suggests, in agreement with the observed rigidochromism, that the dual emission of [W(CO)$_5$(4-NC-pyridine)] originates in two close-lying ^{3}MLCT(4-NC-pyridine) states.

A similar situation occurs in the UV–vis spectra of [M(CO)$_4$(α-diimine)] (M = Cr, Mo, W) complexes [116]: an intense, solvatochromic band in the visible is followed by a weaker solvent-independent band in the near-UV. TD-DFT studies on several such complexes (M = Cr, W; α-diimine = bpy, Me-dab, phen, Me$_4$-phen) confirm the assignment of the lowest band as MLCT(diimine), re-assign the higher band as MLCT(CO) [103,166,170–172] and attribute the dual emission to close-lying ^{3}MLCT(diimine) states [170,171]. The MLCT(diimine) transitions in [M(CO)$_4$(α-diimine)] were shown by both CASSCF [104] and TD-DFT [172] calculations to involve extensive shift of electron density from the CO ligands. Even these transitions, long believed to be prototypical MLCT, should thus be regarded as M,CO → diimine MLLCT. Interestingly, the increase of electron population at the bpy ligand in [Cr(CO)$_4$(bpy)] upon the ^{1}MLLCT transition was calculated [104] to be about the same as that upon 1-electron reduction to [Cr(CO)$_4$(bpy)]$^{\bullet-}$: between 0.7 and 0.8 e$^-$. For M = Cr, irradiation into the lowest absorption band results in ultrafast CO dissociation [116,118,119,154,173,174]. This photoreactivity was explained using CASSCF/CASPT2 and CASSCF/MR-CCI calculations on [Cr(CO)$_4$(bpy)] by mixing (avoided crossing) between potential energy surfaces of ^{1}MLCT(bpy) states and higher-lying ^{1}LF states [29,155].

The DFT studies of mixed-ligand d^6 metal cabonyls discussed above also point to a high degree of covalency, manifested as extensive mixing between metal 'd' and ligand orbitals. As a consequence, the d-character is spread between more orbitals than predicted by LF-type arguments. Thus, for example, the 5dπ contributions to the three highest occupied KS orbitals of [W(CO)$_5$(4-CN-pyridine)] range between 50 and 60%, while at least five high-lying virtual orbitals have a d-content higher than 30%. It follows that traditional arguments of the LF theory cannot be used even for a qualitative discussion of bonding and spectroscopy of these compounds.

CpM(CO)$_2$ (M = Rh, Ir) are interesting complexes, capable of photochemical C–H bond activation [175–177] following an ultrafast CO dissociation [177–179]. In a theoretical study [180], DFT was used to calculate their ground-state structures. Excited-state calculations were performed using the wavefunction SAC-CI method. The most intense UV transition was identified as LMCT Cp → M excitation with a Cp → CO LLCT contribution. A manifold of M,Cp → CO MLLCT states occurs at lower energies. The lowest triplet state involves only small charge redistribution from Cp to M and CO and bending of M–C–O bonds by *ca.* 10° [180]. The excitation-wavelength dependence of the photochemical quantum yield was attributed to different reactivity of individual excited states.

Important insight into excited states of mixed-ligand carbonyls was also obtained using wavefunction-type CASSCF/CASPT2 and CASSCF/MRCI techniques. Detailed theoretical calculations were performed on excited states of the complexes [M(R)(CO)$_3$(H-dab)] (M = Mn, Re; R = H or alkyl) [32–34,181,182], sometimes even including spin-orbit coupling [183]. Results of this work were extensively reviewed [27,31,37,184,185]. Besides assigning UV–vis spectra, these calculations have addressed questions of mixing between MLCT and LLCT states, photochemical roles of SBLCT states, time-dependent population of individual states after laser pulse excitation, or ultrafast photochemical M–R or M–CO bond splitting. CASSCF-type (MRCI, CASPT2) calculations have also contributed significantly to our understanding of spectra, excited states and ultrafast metal–ligand bond splitting in hydrido-carbonyl complexes of Mn, Re, Fe, or Os [28,30,31,186–188]. A remarkable CASSCF/MRCI study [84] of [Re(*t*-styrylpyridine)(CO)$_3$(bpy)]$^+$ has interpreted the photochemical *trans* → *cis* ligand isomerization in a full accord with ultrafast spectroscopic experiments [85].

In another study [36], potential energy surfaces of low-lying singlet excited states of CpMn(CO)$_3$ were calculated by CASSCF/MR-CCI. Absorption spectra were then calculated by wavepacket propagation on excited-state surfaces. Non-adiabatic coupling between states in the region of vertical excitation was found to strongly affect intensities of UV absorption bands. Wavepacket propagation was also used to interpret and predict photochemical outcomes (ionization, fragmentation) of irradiation with shaped femtosecond laser pulses. This is an important step toward laser-driven photochemistry, whereby the yield of the desired product is optimized by controlling the process of excitation [189].

5. Excited states of strongly phosphorescent cyclometallated complexes

Organometallic complexes of heavy metals with C^N-type ligands often show strong phosphorescence with quantum yields higher than 0.1, sometimes even approaching unity. Design, synthesis, characterization, electrochemistry, spectroscopy and photophysics of such compounds comprise a vigorous research area, driven by their possible use in display devices (OLEDs),

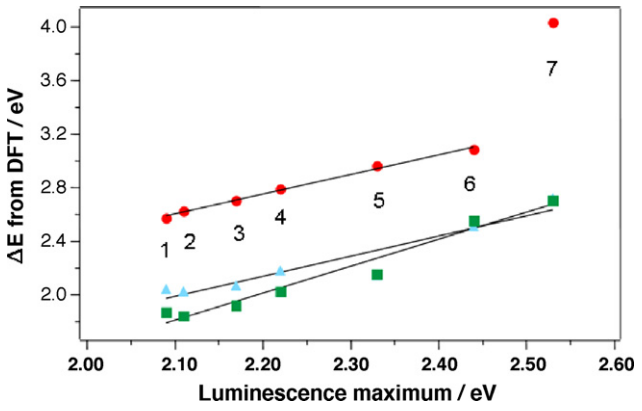

Fig. 13. Correlation between DFT-calculated parameters and maxima of phosphorescence spectral band for a series of $[Ir^{III}(R\text{-mppy})_2(N^\wedge N)]^+$ complexes **1**–**6** (N^N = bpy and its derivatives, R-mppy = 5-methyl-2-(4-R-phenyl)-pyridines). **7**: $[Ir^{III}(F\text{-mppy})_2(dppe)]^+$ (dppe = bis(diphenylphospino)ethylene). Red circles: the HOMO–LUMO gap at optimized singlet geometry. Green squares: the difference of the absolute energy of the triplet state and the ground state at the optimized triplet geometry. Blue triangles: the orbital energy difference of the HSOMO (triplet) and the HOMO (ground state) calculated at the triplet geometry. Adapted from Ref. [192].

probes for biomolecules, reporters of DNA structure or sensitizers. Structural factors leading to the required phosphorescence colors, quantum yields and lifetimes are not entirely understood, presenting challenges and opportunities for theoretical chemistry. The most important and intriguing questions are (i) prediction of triplet energies and phosphorescence wavelengths, (ii) understanding the character of the emissive triplet states, (iii) prediction of radiative decay rate constants k_r, (iv) prediction of nonradiative decay rate constants k_{nr}, (iv) effects of the environment surrounding the chromophore, and (v) effects of the strong electric field present in real devices such as OLEDs. Calculations of vibronic structure and phosphorescence bandwidths would allow us to asses the spectral purity. It would be also important to predict structures and stabilities of one-electron oxidized and reduced forms of the luminophores, which are transiently produced in display devices. Moreover, understanding their electronic structures could help us to understand the formation of phosphorescent triplet states by electron–hole recombination and optimize thus its efficiency. Applications of DFT and TD-DFT to phosphorescent organometallics [190–200] are rather scarce. Theoretical conclusions are often limited to the description and energies of the HOMO and LUMO, and the lowest triplet states calculated by UKS, usually neglecting the solvent.

Fig. 13 compares three different estimates [192] of phosphorescence energies in a series of $[Ir^{III}(C^\wedge N)_2(N^\wedge N)]^+$ complexes, where the emissive states seem to have a mixed Ir → bpy ^{3}MLCT/^{3}ILCT(ppy) character [192,201]. (ILCT stands for intraligand charge transfer, whereby the electron density is transferred from the phenyl to the pyridine part of the C^N ligand.) Simple LUMO–HOMO energy difference at the ground-state geometry (red circles) affords a good correlation for the compounds **1**–**6**, but the absolute values are much higher than the experimental ones. The correlation breaks down for the compound **7**, where the excited-state is purely $\pi\pi^*$(F-mppy) ^{3}IL, with a different singlet–triplet splitting. Good results were obtained using energy differences between the lowest triplet state and the ground state calculated at the relaxed triplet geometry (green squares). Differences between the energies of the highest singly occupied orbital (HSOMO) of the triplet and the HOMO of the ground state (blue triangles, both calculated at the triplet geometry) also yield a good correlation. A similar approach, where the HSOMO–HOMO differences were calculated at the ground-state geometry, was successfully used to estimate the phosphorescence energy in [Pt(ppy)(acac)] [190], or *fac*- and *mer*-isomers of $[Ir(ppz)_3]$ (ppz = 1-phenyl-pyrazolyl, another C^N ligand) [199]. All these approaches, however, suffer from the neglect of spin-orbit coupling, which could shift the calculated triplets and singlets to lower and higher energies, respectively [191], and of medium effects.

$[Ir(2\text{-}(2,4\text{-}F_2\text{-phenyl})\text{-}5\text{-}CF_3\text{-pyridine})_2(4,4'\text{-}Bu^t_2\text{-bpy})]^+$ is an exceptionally strong emitter among the $[Ir(C^\wedge N)_2(N^\wedge N)]^+$ complexes [200]. DFT calculations of its KS orbitals have shown [200] that LUMO and LUMO + 1 lie close in energy, being localized on the N^N and C^N ligands, respectively. This explains why this complex is reducible in two successive one-electron steps while only single reduction was seen for other $[Ir(ppy)(N^\wedge N)]^+$ complexes. Introduction of fluoro groups to the ppy ligand strongly stabilizes its π^* orbitals. The high emission quantum yield cannot, however, be explained by DFT-MO calculations alone, without understanding the mechanism of the excited-state deactivation.

TD-DFT was employed to calculate singlet and triplet transitions for $[Ir(ppy)]_3$, $[Ir(ppy)_2(acac)]$, and $[Ir(ppy)_2(bza)]$, (ppy = 2-phenylpyridine, acac = acetylacetonate, bza = benzoylacetonate $PhC(=O)CHC(=O)Me^-$) [191]. Calculated lowest singlet transitions and triplet energies compare well with experimental absorption and phosphorescence band maxima, even if calculated at the ground-state geometry and neglecting the medium. DFT calculations also reveal interesting aspects of the characters of emissive excited states. The HOMO of most cyclometallated complexes is composed from 40 to 70% of metal dπ orbitals. π orbitals of the ppy phenyl groups are the next most important contribution. The LUMO is either predominantly localized on the pyridyl part of the ppy-type ligands or on other ligands present in the coordination sphere. Metal contribution to the LUMO is usually negligible. Depending on the particular compound, MLCT, LLCT, IL($\pi\pi^*$), or ILCT characters mix in the emissive lowest triplet state. The emissive state of the prototypical tris-cyclometallated complex $[Ir(ppy)_3]$ was described as ^{3}MLCT [191]. However, the large (∼40%) π admixture to the high-lying occupied orbitals points to a mixed ^{3}MLCT-IL, or (better) ^{3}MLCT-ILCT character, whereby the electron density is transferred into the pyridine parts of the ppy ligands from the Ir atom as well as from the phenyl parts of the ligands. Difference electron density maps that would describe the excited states more precisely are not available. Neither were addressed more subtle questions such as delocalization of the excitation over the three equivalent ligands. A similar character was determined by UKS [191] for the phosphorescent state of $[Ir(ppy)_2(acac)]$, where the calculated spin densities are 0.57 (Ir), ∼0.7 (each ppy) and 0.04 (acac). The situation is less clear for $[Ir(ppy)_2(bza)]$ whose LUMO is

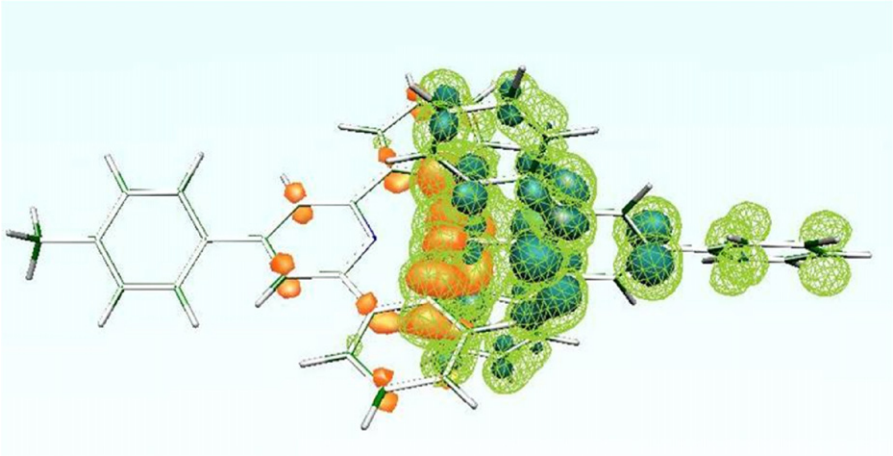

Fig. 14. The spin density (green chicken wire), the lower SOMO (LSOMO, orange) and the HSOMO (emerald) in the lowest triplet state of a $[Ir(C^N^C)(N^N^N)]^+$ complex. LSOMO and HSOMO approximately correspond to the hole and electron created upon excitation. From Ref. [194].

localized at the bza ligand. The very close energetic proximity of Ir → ppy ^{3}MLCT/^{3}ILCT(ppy) and Ir,ppy → bza ^{3}MLLCT states (TD-DFT at the ground-state geometry) does not allow us to decide on the real nature of the lowest relaxed triplet state.

The 1-phenylpyrazolyl (ppz) ligand is a weaker electron acceptor than ppy. Hence, $[Ir(R\text{-}ppz)_3]$ complexes are not reducible and, with the exception of *fac*-$[Ir(CF_3\text{-}ppz)_3]$ are emissive only in low-temperature glasses [199]. The lowest triplet state of $[Ir(ppz)_3]$ is ^{3}ILCT/MLCT, the electron density being shifted from the phenyl parts of the ligand and, partly, the Ir atom to the pyrazolyl units [199]. The HOMO is delocalized over three or two ppz ligands in the *fac*- and *mer*-isomers, respectively. The π^*(ppz) LUMO is delocalized over three ppz ligands in the *fac*-isomer, while it is localized on a single ligand in the *mer*-isomer.

MLLCT or even LLCT characters of phosphorescent excited states are common in some mixed-ligand cyclometallated complexes. For example, UKS spin-density distribution in the lowest triplet of $[Ir(ppz)_2(bpy)]^+$, together with the shapes of the HOMO and LUMO, show that electron density is transferred from the phenyl rings of ppz ligands and the 5dπ(Ir) orbital to π^*(bpy). This indicates an Ir,ph(ppz) → bpy ^{3}MLLCT character of the emissive state [195]. Moreover, it has been noted [195] that the HOMO and LUMO orbitals in $[Ir(ppz)_2(bpy)]^+$ are essentially orthogonal and, thus, little interacting. This means that the HOMO and LUMO energies can be tuned almost independently by varying the substituents on the ppz- and the bpy-type ligands, respectively, resulting in tuning of both the singlet and triplet MLLCT energies over a broad range [195]. Accordingly, the energy of the lowest allowed singlet MLLCT transition in the $[Ir(R\text{-}ppz)_2(N^N)]^+$ series shows nearly 1:1 linear correlation with the redox gap $E^{ox}_{1/2} - E^{red}_{1/2}$ [195].

An interesting LLCT excited state was revealed by DFT for $[Ir(C^N^C)(N^N^N)]^+$, where C^N^C are derivatives of 2,5-diphenylpyridine and N^N^N are terpyridine-type ligands [194]. Figs. 14 and 15 show that the electron density is transferred from the C^N^C to the N^N^N ligand, the reorganization of the electron density being the largest in the region around the Ir atom. The phosphorescence quantum yield from this state is rather low, 0.027–0.035, depending on the particular compound [194].

Analysis of DFT-calculated HOMO and LUMO and a TD-DFT calculation (at ground-state geometry) of mixed-

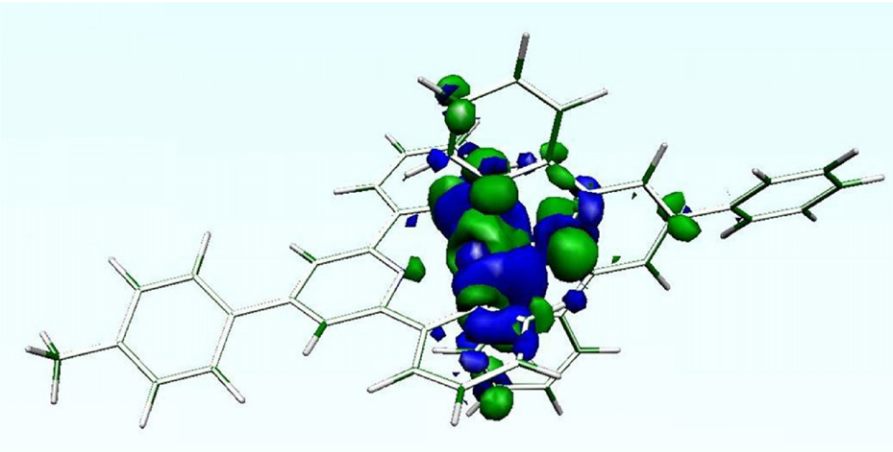

Fig. 15. Electron-density difference between the lowest triplet and the ground state of a $[Ir(C^N^C)(N^N^N)]^+$ complex. The blue and green areas correspond to the regions of decreased and increased electron density upon excitation, respectively. From Ref. [194].

ligand cyclometallated Rh(III) complexes $[Rh(ppy)_2(TAP)]^+$ and $[Rh(thpy)_2(TAP)]^+$ (thpy = 2,2′-thienylpyridine (a C^N-type ligand), TAP = 1,4,5,8-tetraazaphenanthrene, a strong π electron acceptor) have identified their lowest triplet states as MLLCT, involving a charge transfer from C^N to TAP [193]. A dual phosphorescence was observed for $[Rh(thpy)_2(TAP)]^+$ in a 77 K glass and has been assigned, using TD-DFT, to the lowest ^{3}MLLCT state and a higher-lying ^{3}IL(thpy) state [193].

HOMO and LUMO were also analyzed for planar Pt complexes of the type [Pt(C^N)(O^O)], where O^O is a β-diketonate. A Pt → C^N MLCT character seems to predominate in the lowest triplet, mixed with O^O → C^N LLCT and C^N ILCT contributions [190].

$[Os(Cl)(CO)_3(O^O)]$ constitute another class of highly phosphorescent complexes. Depending on the β-diketonate ligand O^O, the phosphorescence quantum yields can approach unity [196]. This is the case of complexes containing asymmetric O^O ligand (2-naphthyl)–C(=O)–CH–C(=O)-(7-*N*,*N*-dimethylaniline). TD-DFT has shown that the lowest allowed singlet transition corresponds to a HOMO → LUMO excitation, which amounts to an ILCT from the dimethylaniline unit to the C(=O)–CH–C(=O) moiety [196]. The lowest relaxed triplet (UKS) originates in 90% HOMO → LUMO ILCT with a 10% HOMO − 1 → LUMO admixture, which introduces minor naphthyl → C(=O)–CH–C(=O) ILCT and $\pi\pi^*$ contributions [196]. Pronounced solvatochromism of these complexes indicates large dipole-moment changes upon excitation. Indeed, values of 18.0 and 11.9 D were calculated for singlet and triplet excitation, respectively [196]. Obviously, full theoretical treatment of these states would require to include the solvent. The origin of the emission from similar complexes $[Os(CF_3COO)(CO)_3(O^O)]$ (O^O = R–C(=O)–CH–C(=O)–CF_3) depends on the group R [198]. DFT-calculated HOMO and LUMO indicate [198] predominantly $^3\pi\pi^*$ IL(O^O) character mixed with an $Os(CF_3COO)$ → O^O ^{3}MLLCT contribution, which decreases in the order R = CF_3 > *t*Bu > phenyl > naphthyl > anthryl. Fluorescence from a $^1\pi\pi^*$ state was seen [198] for R = pyrenyl.

Given the practical potential of phosphorescent states of these organometallics, it is surprising that their in-depth theoretical analyses are still missing, at least to the author's knowledge. The DFT or TD-DFT descriptions of phosphorescent excited states discussed above are supported by a generally good agreement of experimental absorption spectra with calculated singlet transitions. Calculated triplet energies usually agree reasonably well with emission spectra. Nevertheless, limiting the excited-state description to HOMO/LUMO characters, calculating phosphorescent triplets at ground-state geometries and neglecting the medium could easily lead to erroneous results. One can wonder whether the calculated ILCT or LLCT contributions to emissive states are not exaggerated by neglecting the solvent. Important questions such as the vibronic structure of phosphorescent bands and decay rates and mechanisms were not yet addressed by quantum-chemical calculations. The observation [192] that nonradiative rate constants in a large series of cyclometallated Ir(III) complexes follow the energy-gap law suggests that phosphorescence lifetimes could be discussed in terms of calculable parameters. However, understanding of the decay mechanisms would require a detailed examination of the excited state manifold to account for relaxation through "dark" states (Section 3.4). Intervention of such states has been indicated [190,202] for the decay of higher excited states of [Pt(C^N)(O^O)]. Moreover, it is necessary to consider splitting of triplet levels to spin-orbit components, each of which decays with an unique radiative and nonradiative rate constant. Most importantly, spin-orbit coupling provides for the non-zero intensity of the, formally, spin-forbidden triplet → singlet phosphorescence. A TD-DFT-SOC method, which includes spin-orbit coupling, has been developed and first applications are emerging [4,5].

6. Ruthenium-polypyridine sensitizers of solar energy conversion

Irradiation of nanostructured TiO_2 electrodes covered with a monolayer of adsorbed Ru(II) polypyridine complexes results in an ultrafast electron injection from electronically excited states of the Ru sensitizer into the TiO_2 conduction band. This is the operational principle of the Grätzel photoelectrochemical cell, which converts solar energy to electrical energy [203–208]. $[Ru(4,4'\text{-}(COOH)_2\text{-}2,2'\text{-}bpy)_2(NCS)_2]$ (abbreviated N3) is the generic photosensitizer, whose derivatives are used even in the most recent high-performance versions of Grätzel solar cells [208]. Development of new, efficient and durable Ru sensitizers continues and, in principle, can be guided by theory.

Photosensitization of nanoparticles by molecular dyes presents many challenges for quantum-chemical calculations. In the particular case of TiO_2 photosensitization, it is first necessary to understand the excited-state characters of the Ru polypyridine complexes and their energies relative to the TiO_2 conduction band [47,76,88,209–212]. Propensity of the excited states to electron injection needs to be assessed by careful examination of their localization on those regions of the sensitizer molecule which interact with the semiconductor surface. The whole manifold of energetically relevant excited states, singlets and triplets, has to be investigated, since electron injection can take place also from upper states, competitively with their relaxation. The ultimate goal, however, is to understand the structures and excited states of the sensitizer-TiO_2 assemblies [47,213,214]. A very interesting question arises; to which extent are the molecular excited states of the sensitizer delocalized onto the semiconductor nanoparticle. The answer determines whether the electron injection occurs sequentially, as an ultrafast electron transfer following optical excitation, or as a direct optical charge transfer from the sensitizer to the semiconductor.

DFT and TD-DFT techniques were applied to the $[Ru(bpy)_2(NCS)_2]$ model and its analogues $[M(bpy)_2(L)_2]$ (M = Ru, Os; L = NCS, CN) [88], the N3 sensitizer $[Ru(4,4'\text{-}(COOH)_2\text{-}2,2'\text{-}bpy)_2(NCS)_2]$ [209,210,212], its deprotonated forms [76,210–212], and a related sensitizer $[Ru(4,4'\text{-}(COOH)_2\text{-}2,2'\text{-}bpy)(4,4'\text{-}Me_2\text{-}2,2'\text{-}bpy)(NCS)_2]$ [212]. All these calculations underlie the importance of including the solvent. It was found that the polar solvent increases the polarity of the ground-state solute molecule $[M(bpy)_2(NCS)_2]$ by sta-

bilizing the $[(M(bpy)_2^{2+})(NCS^-)_2]$ resonance form. On going from the vacuum to the solution, the M-N(bpy) and M-NCS bond lengths increase and decrease, respectively. Presumably, this is caused by diminishing the Ru → bpy π back donation and strengthening SCN → Ru σ and π donation, respectively [88]. Similar conclusion emerged from a DFT study [209] of $[Ru(4,4'\text{-}(COOH)_2\text{-}2,2'\text{-}bpy)_2(NCS)_2]$, which calculated the ground-state dipole moments of 10.93, 19.81, and 20.60 D in the vacuum, EtOH and H_2O, respectively. All published DFT calculations have identified two sets of occupied MOs, which have a mixed 4dπ(Ru)/π(NCS) character. Ru-NCS π bonding and NCS-localized orbitals lie lower, followed by Ru-NCS π antibonding HOMOs. The hybrid functionals B3LYP or PBE0 lead to larger 4dπ participation in HOMOs than "pure" functionals [209], which exaggerate the NCS^- contribution. The six lowest-lying unoccupied MOs of $[Ru(4,4'\text{-}(COOH)_2\text{-}2,2'\text{-}bpy)_2(NCS)_2]$ are π*(bpy) in character, with considerable contributions from the COOH groups.

Electronic absorption spectra of $[Ru(4,4'\text{-}(COOH)_2\text{-}2,2'\text{-}bpy)_2(NCS)_2]$ and $[Ru(bpy)_2(NCS)_2]$ are generally well reproduced by TD-DFT calculations, but only if the solvent is included. Vacuum calculations underestimate the energy of the lowest allowed singlet transitions, as well as the lowest triplet energy. The solvatochromism being larger for the lower-lying transitions, the vacuum calculations exaggerate the separation between spectral bands relative to solution spectra.

The spectrum of $[Ru(4,4'\text{-}(COOH)_2\text{-}2,2'\text{-}bpy)_2(NCS)_2]$ consists of two bands in the visible spectral region, which were both calculated to originate in MLLCT transitions from the $Ru(NCS)_2$ moiety to the $4,4'\text{-}(COOH)_2\text{-}2,2'$-bpy ligand(s). A third band, due to ππ*(bpy) IL transitions, occurs at higher energy, in the near UV [209,210]. Most of the transitions have a highly mixed character, combining several one-electron excitations. In particular, TD-DFT shows that the transitions responsible for the first and second visible spectral bands originate in the Ru-NCS π antibonding and bonding orbitals, respectively. They all terminate in the LUMO and other low-lying π* virtual orbitals of the $4,4'\text{-}(COOH)_2\text{-}2,2'$-bpy ligands. Delocalization of the excited electron over the –COOH groups, which interact with the TiO_2 surface, is instrumental for the electron injection [209]. The partial localization of the positive "hole" on NCS^- ligands is preserved in the oxidized state $[Ru^{III}(4,4'\text{-}(COOH)_2\text{-}2,2'\text{-}bpy)_2(NCS)_2]^+$. This could be an important factor facilitating reduction of the oxidized sensitizer that is essential for a good performance of a solar cell. All studies point to a large density of excited states, which can be of importance for efficient electron injection into the TiO_2 conduction band. Deprotonation of the carboxylic groups results in a blue shift of the absorption bands, which was well reproduced by TD-DFT (B3LYP) in an aqueous solvent [210,212]. The MLLCT character of the transitions responsible for the two lowest absorption bands is preserved upon deprotonation, although their orbital origins are somewhat different [210]. A vacuum calculation (B3LYP) of $[Ru(4,4'\text{-}(COO^-)_2\text{-}2,2'\text{-}bpy)_2(NCS)_2]^{4-}$ has predicted [76] low-lying ILCT transitions transferring electron density from the COO^- groups to the bpy π* system. However, these states were not identified in calculations performed in a solvent [210,211]. It seems that TD-DFT in vacuum underestimates energies of COO^- → bpy ILCT transitions due its deficiency in describing long-range CT (Section 2.4). Solvatochromism of $[Ru(4,4'\text{-}(COOH)_2\text{-}2,2'\text{-}bpy)_2(NCS)_2]$ was satisfactorily modeled by CPCM, which accounts well even for the small spectral blue shift on changing the solvent from EtOH to H_2O that is caused by the slightly larger difference between the ground- and excited-state dipole moments in more polar H_2O. Indeed, it was estimated [209] that the dipole moment of $[Ru(4,4'\text{-}(COOH)_2\text{-}2,2'\text{-}bpy)_2(NCS)_2]$ decreases upon the lowest allowed MLLCT transition (approximated by HOMO → LUMO excitation) by 5.67, 10.25, and 10.49 D in the vacuum, EtOH and H_2O, respectively. Surprisingly, the computational studies published so far paid no attention to triplet states of Ru sensitizers, despite their, experimentally proven, role in electron injection.

A detailed DFT/TD-DFT computational study [212] of N3 and $[Ru(4,4'\text{-}(COOH)_2\text{-}2,2'\text{-}bpy)(4,4'\text{-}Me_2\text{-}bpy)(NCS)_2]$ (a model for the N621 sensitizer) has investigated effects of protonation of terminal carboxylate groups on electronic transitions and molecular orbitals and their energy matching with the conduction band of a TiO_2 nanoparticle that was modeled by $(TiO_2)_{38}$. The solvent was included in the calculations and, for the deprotonated forms, the counterion was considered explicitly, modeled by Na^+. Several suggestions for designing efficient sensitizers were drawn, namely that (i) deprotonation decreases the light-harvesting ability by increasing the transition energies and (ii) di- and monoprotonated forms represent the best trade-off between the light harvesting ability and energetic match between excited states and the TiO_2 conduction band. The two lowest absorption bands were confirmed to belong to $Ru(NCS)_2$ → bpy MLLCT transitions, the higher one with a small contribution from LF excitation.

A few studies have addressed the questions of geometric and electronic structures of whole sensitizer–TiO_2 assemblies [213,214]. The semiconductor nanoparticle was modeled by a $(TiO_2)_{38}$ cluster of an anatase structure, with the (1 0 1) surface exposed to the sensitizer molecule. The DFT-optimized (B3LYP, vacuum) structure of $[Ru(4,4'\text{-}(COOH)_2\text{-}2,2'\text{-}bpy)_2(NCS)_2]/(TiO_2)_{38}$ shows [213] that the sensitizer is bound to Ti atoms by two COO groups of a single ligand. The S atom of one of the NCS ligands is surprisingly close (3.5 Å) to the TiO_2 surface. Importantly, it was found that the nanoparticle and the sensitizer molecule undergo significant structural adjustments upon binding, to provide for strong mutual interaction. These involve twisting the COO groups and displacing the bound Ti atoms outwards, above the nanoparticle surface. The HOMO and other high-lying occupied MOs have the same mixed 4dπ(Ru)/π(NCS) character as in the isolated sensitizer molecule. The LUMO is from 86% localized on that $4,4'\text{-}(COO^-)_2\text{-}2,2'$-bpy ligand, which is bound to TiO_2. Conjugated TiO_2 orbitals contribute the remaining 14%. LUMO + 1 is localized on the unbound $4,4'\text{-}(COOH)_2\text{-}2,2'$-bpy. Other virtual MOs, which follow close in energy, have contributions from $4,4'\text{-}(COO^-)_2\text{-}2,2'$-bpy ligands as well as the $(TiO_2)_{38}$ cluster. The formidable size of the system limited the TD-DFT calculation to the three lowest singlet transitions. The calculated transition energies are heavily underestimated; the neglect of the solvent

being one of the reasons. The transitions are composed of several one-electron excitations, the most prominent (38–46%) component being MLLCT, predominantly localized on the sensitizer molecule. They are directed to low-lying MOs, many of which are coupled with nanoparticle orbitals. The strength of this coupling is different for different sensitizer excited states, depending on the energy and localization of the orbital(s) populated. Consequently, electron injection is expected to follow multiexponential dynamics, possibly dependent on the excitation wavelength. This predicted behavior essentially agrees with experiments.

The second study [214] has addressed the question of delocalized sensitizer-to-nanoparticle transitions in $[Fe(CN)_6]^{4-}$/$(TiO_2)_{38}$ assembly. Its structure was optimized in vacuum using the Car–Parrinello combined DFT/MD approach [215] employing a pure PBE functional. Electronic transitions were then calculated by TD-DFT with the B3LYP functional in water, described by CPCM. The size of the system has limited the TD-DFT calculation to the 12 lowest states. Hence, to simulate the absorption spectrum, the transition energies were approximated by orbital energy differences. A real $[Fe(CN)_6]^{4-}$/TiO_2 system in an aqueous solution shows a band at ~420 nm, that is seen neither in the spectrum of isolated $[Fe(CN)_6]^{4-}$ nor TiO_2. The simulated spectrum agrees reasonably well with the experiment. Several transitions contributing to the ~420 nm band were identified computationally as excitations from $3d_\pi$(Fe) orbitals to empty orbitals of $(TiO_2)_{38}$. The most intense transitions are directed to the orbitals predominantly localized on that Ti atom to which $[Fe(CN)_6]^{4-}$ is linked, with small contributions from neighboring Ti atoms. These transitions are called MPCT, metal to particle charge transfer [214].

In this respect, it is necessary to mention the combined DFT/MD study of a catecholate/$(TiO_2)_{38}$ adduct [216]. Comparison of the DFT calculations of the $[Ru(4,4'\text{-}(COOH)_2\text{-}2,2'\text{-bpy})_2(NCS)_2]$/$(TiO_2)_{38}$, $[Fe(CN)_6]^{4-}$/$(TiO_2)_{38}$ and catecholate/$(TiO_2)_{38}$ systems shows that the lowest excited state can range from "molecular", that is sensitizer-localized MLLCT, to a delocalized MPCT, pertinent to the whole assembly. The present Grätzel-type solar cells operate on sensitizer-localized transitions that are followed by ultrafast electron injection. It is possible that this approach is superior to a direct optical charge transfer into the semiconductor, because of a much slower rate of the back electron transfer. However, it remains to be shown whether this is really the case, and whether MPCT states could be employed in efficient light energy conversion. It also follows that DFT has a great potential to calculate molecule-nanoparticle assemblies, predict their properties and dynamic behavior.

7. Ru^{II}-polypyridine complexes and the $[Ru(phen)_2(dppz)]^{2+}$ light switch

The prototype photosensitizer $[Ru(bpy)_3]^{2+}$ still awaits its detailed TD-DFT investigation that would address the nature and, especially, the localization of the lowest excited state. Previous DFT studies [217,218] (pure functionals, vacuum) have well reproduced the absorption spectrum and identified the lowest transitions as MLCT. Spin-orbit calculations [217] have indicated a substantial mixing between triplet and singlet states. DFT calculation [218] also found that energies of ^{1,3}LF states, which lie almost 2 eV above the lowest ^{1,3}MLCT states at the ground-state geometry, drop rapidly with increasing the Ru–N distance. This leads to mixing between ^{3}MLCT and ^{3}LF states, which results in a low-yield, thermally activated [219] photochemical Ru–N bond cleavage.

An UKS calculation (B3LYP, vacuum) [72] has identified the lowest triplet excited state of $[Ru(bpy)_3]^{2+}$ as a delocalized $^3A_2$ and established the nature and ordering of its spin-orbitals. Moreover, an excited-state absorption spectrum of $[Ru(bpy)_3]^{2+}$ was obtained by a TD-DFT open-shell calculation performed on the $^3A_2$ state. It matches well the experimental excited-state spectrum [220] and assigns it [72] to IL and mixed LMCT/LF transitions. The latter are clearly identified by comparison with the spectrum of $[Ru(bpy)_3]^{3+}$, which was also assigned [72] using TD-DFT. In this respect, it is interesting to note that the TD-DFT calculation assumed a D_3 symmetry of the excited complex and delocalization of the excited electron over all three bpy ligands, that is $^*[Ru^{III}(bpy^{-1/3})_3]^{2+}$, whereas the experimental spectrum was empirically interpreted [220] as an evidence for a localized character of the excited state; $^*[Ru^{III}(bpy)_2(bpy^{\bullet-})]^{2+}$. Obviously, the excited-state spectrum does not necessarily imply localization of the excited electron and cannot distinguish between the localized and delocalized structures. To the author's knowledge, this is the first application of open-shell TD-DFT to excited-state electronic spectra of a transition-metal complex. It demonstrates the great potential of TD-DFT to interpret excited-state spectra and facilitate identification of short-lived electronically excited species by time-resolved UV–vis spectroscopy.

TD-DFT has been successfully used to calculate CD spectra of $[Ru(phen)_3]^{2+}$ and its Os and Fe analogues over the whole UV–vis spectral range [221]. Very good match with experimental spectra was achieved for Ru and Os, using pure functionals. The lowest set of transitions is MLCT, directed into an a_2 orbital that is delocalized over the three phen ligands. Incorporation of the aqueous solvent (COSMO) has a negligible effect, as was demonstrated for Os. The agreement with experiment is worse for the lowest CD MLCT band of $[Fe(bpy)_3]^{2+}$, where the best results were obtained using BP86 TD-DFT on B3LYP-optimized structure [221]. Subtle electronic and structural effects apparently arise from the close proximity of MLCT and LF states in $[Fe^{II}(phen)_3]^{2+}$.

Interesting case is presented by $[Ru(bpy)_2(LH_2)]^{2+}$, where LH_2 is a phen ligand with an appended Shiff base containing two phenol groups: *N*,*N*′-bis(salicylidene)-1,10-phenanthroline-diamine [72,222]. It shows a very unusual photophysics, whereby the ^{3}MLCT emission is rapidly quenched to produce another excited state, which is nonemissive but very long-lived (30 μs) [222]. DFT calculations (B3LYP, vacuum) [72] have shown that several occupied phenol-based orbitals occur above dπ(Ru), becoming the HOMOs. TD-DFT calculations [72] have identified a manifold of low-lying ILCT and LLCT transitions which involve electron excitation from phenol orbitals to the phen moiety or to the distant bpy ligands, respectively. These transitions are very weak, not manifested in the electronic absorption spectrum. The corresponding ^{3}ILCT and ^{3}LLCT

states lie below the usual ^{3}MLCT states. It was suggested [72] that the ^{3}MLCT state undergoes a rapid conversion to the ^{3}ILCT state(s), which are long-lived. This interesting suggestion again demonstrates the ability of TD-DFT to identify spectroscopically silent but photophysically important excited states. However, the TD-DFT conclusions have to be accepted with caution, because of the neglect of the solvent. Although the results are probably correct for ILCT states, the energies of the long-range LLCT transitions and triplet states can be strongly underestimated, see Section 2.4.

Oligonuclear Ru^{II} polypyridine complexes are being developed as "molecular wires" for electron or energy transfer. Very interesting complexes of this type are based on a tppz ligand (tetra-2-pyridyl-1,4-pyrazine), which can serve both as a bridging and terminal ligand. Complexes of the type $[Ru_n(tppz)_{n+1}]^{2n+}$ and $[tpy_2Ru_n(tppz)_{n-1}]^{2n+}$ were made and investigated spectroscopically and electrochemically. DFT calculations [223,224] have shown that the HOMO–LUMO gap in the ground state rapidly decreases with the increasing chain length n and the oligomers attain a quasi-band electronic structure for $n > 3$ [223] and the effective electronic conjugation length, at which the spectral properties no longer depend on the chain length, was estimated [224] as $n > 5$. For shorter oligomers, the lowest absorption band of $[Ru_n(tppz)_{n+1}]^{2n+}$ shifts to longer wavelength and becomes more intense with increasing n. TD-DFT calculations [224] have reproduced this behavior and identified the main transitions. They involve excitations from predominantly dπ(Ru) orbitals of several Ru centers into MO's, which are composed predominantly of π^*(bridging tppz) orbitals, with smaller, but still significant, dπ(Ru) contributions. Such transitions are delocalized over the whole oligomers. They can be viewed as partly Ru → bridging tppz MLCT mixed with π(RuN) → π^*(RuN) transitions of the Ru(bridging tppz)Ru units. (Note that similar transitions were established for mononuclear $[W(CO)_4$(aryl-dab)] complexes with strong M → dab π back bonding [106].) These transitions are followed in energy by MLCT from dπ(Ru) to π^*(tppz) orbitals localized on the pyridyl moieties. IL $\pi\pi^*$ transitions occur further in the UV. Based on their electronic structures, Ru(tppz) oligomers are expected to show a band-like hole conduction [223]. Methodologically, it is interesting to note that the oligomer structures were optimized [224] using the DFT within the Car-Parrinello molecular dynamics method [215] and a GGA-type functional. The following TD-DFT calculation employed the hybrid B3LYP functional and a CPCM treatment of the solvent. It has been noted [223] that further theoretical studies of these highly charged oligomers will have to include the counterions explicitly.

$[Ru(phen)_2(dppz)]^{2+}$ (dppz = dipyrido[2,3-a:3′,2′-c]phenazine) is much studied as a "light-switch", whose emission is strongly medium-dependent. The dppz ligand is often viewed as a superposition of phen and phenazine moieties. It sticks out of the complex molecule and can intercalate into DNA. $[Ru(phen)_2(dppz)]^{2+}$ is non-emissive in water but shows a strong emission in aprotic solvents or in adducts with DNA. This and related complexes are thus explored as probes of the DNA structure and function. Explanations proposed for the "light-switching" effect assume the presence of several excited states whose relative energies depend on the medium. Two different Ru → dppz MLCT states involving the phen and phenazine moieties, Ru → phen MLCT and IL(dppz) excited states were considered. Recently, a series of interesting TD-DFT studies on the nature of the low-lying states in dppz complexes emerged [101,225,226]. Other investigations attempted to calculate vibrational spectra of Ru^{II}, Re^{I} or Cu^{I} dppz complexes, the dppz ligand and its radical-anion, aiming at interpretation of ground- and excited-state resonance Raman spectra [227,228].

TD-DFT calculation (B3LYP) of singlet transitions in $[Ru(phen)_2(dppz)]^{2+}$ performed in solution (CH_3CN, H_2O) assign the lowest broad absorption band at about 440 nm as originating in two groups of transitions, which are composed of 4dπ(Ru) → π^*(dppz) and 4dπ(Ru) → phen excitations [225]. The third group, due to predominantly $\pi\pi^*$ IL(dppz) transitions, gives rise to a narrow band at ∼375 nm. The dppz π^* orbital populated upon these transitions is mostly localized on the phenazine part [225]. Triplet states were studied for $[Ru(bpy)_2(dppz)]^{2+}$ by TD-DFT and DFT (B3LYP) in vacuum, EtOH and H_2O [101]. To account for hydrogen bonding with the two uncoordinated dppz nitrogens in water, an adduct $\{[Ru(bpy)_2(dppz)]\cdot 2H_2O\}^{2+}$ was calculated as a single entity and placed into a high-dielectric solvent EtOH that was modeled by CPCM-type continuum model. Because of their different symmetries, it was possible to calculate and optimize separately the lowest ^{3}MLCT and ^{3}IL(dppz) states. They are nicely represented by NTOs (Section 2.7) Relaxed $^3\pi\pi^*$ ^{3}IL(dppz) state was calculated to be the lowest excited state of $[Ru(bpy)_2(dppz)]^{2+}$ and $[Ru(bpy)_2(dppz)(H_2O)_2]^{2+}$ in vacuum and low-dielectric media, $\varepsilon < 4$. It is followed in energy by two ^{3}MLCT(bpy) states and, at higher energy, by ^{3}MLCT(dppz). The situation is different for $[Ru(bpy)_2(dppz)(H_2O)_2]^{2+}$ in high-dielectric media (EtOH), where ^{3}MLCT(dppz) is the lowest excited state, which is quasidegenerate with $^3\pi\pi^*$ ^{3}IL(dppz) [101]. No conclusions on the detailed nature of the ^{3}MLCT(dppz) state can be drawn since NTO's were not presented. From this study, one may conclude ^{3}IL(dppz) to be the bright state in aprotic and nonpolar media, the "light-switching" effect originating in the stabilization of ^{3}MLCT(dppz) upon protonation and increasing the medium polarity. However, the authors suggest ^{3}MLCT(dppz) to be the bright state, based on spin-orbit arguments [101].

The situation may be profoundly different when $[Ru(phen)_2(dppz)]^{2+}$ is intercalated into DNA. In a seminal study [226], the structure of a complex between $[Ru(phen)_2(dppz)]^{2+}$ and adenine–thymine tetramer, including 32 water molecules and 8 Na^+ counterions, was optimized. Using the structural parameters of this larger entity, a TD-DFT (B3LYP) calculation was performed on a smaller complex between $[Ru(phen)_2(dppz)]^{2+}$ and an adenine–thymine dimer in water. Surprisingly, occupied orbitals of adenine and thymine were found to lie above 4dπ(Ru) orbitals. The three lowest allowed transitions have predominant contributions from adenine/thymine → dppz/phen CT excitations. The three lowest triplet states were calculated [225] to originate in mixed adenine/thymine → dppz/phen and Ru → dppz/phen excitations. These conclusions are supported by a good match between the calculated absorption and emis-

sion spectra and those measured for $[Ru(phen)_2(dppz)]^{2+}$–DNA complexes. In general terms, this study underlines the importance of calculating explicitly the whole supramolecular assemblies, as opposed to limiting theoretical investigations to their components. It follows that CT excitations between the medium and embedded chromophores can have important spectroscopic and photophysical consequences. These are very important points for designing photonic systems based on supramolecules or molecule/nanoparticle assemblies.

8. Absorption spectra, photophysics, and photochemistry of Re(I) and Ru(II) isonitrile complexes

Singlet excitations of a series of complexes of 2,6-dimethylphenylisocyanide (abbreviated CNx) were analyzed using TD-DFT (B3LYP/CPCM). Simulated spectra correspond very well to experimental ones measured in various solvents. The corresponding triplet states were modeled by UKS. Higher triplets were calculated by TD-DFT at the optimized geometry of the lowest triplet [114,229–231], neglecting structural differences between triplets of different orbital origin. Characters of the transitions and excited states were discussed using the KS orbitals involved.

These studies further support the delocalized view of CT electronic transitions. The lowest allowed transitions of $[Ru(bpy)_2(CNx)Cl]^+$ have Ru,CNx → bpy and Ru,Cl → bpy MLLCT characters [114,229]. Ru,Cl → CNx MLLCT transitions occur at higher energies. For $[Ru(bpy)_2(CNx)_2]^{2+}$, the lowest transitions were identified as predominantly Ru,CNx → bpy MLLCT, while those of $[Ru(bpy)_2(CNx)(py)]^{2+}$ look more like Ru → bpy MLCT. The lowest triplet in all these complexes was found (in vacuum) to be essentially Ru → bpy MLCT [229]. It is closely followed in energy by triplets with a large LF contribution or, for the chloro complex, $\pi\pi^*$ IL(bpy). The LF states lie close enough to be thermally populated, providing a deactivation pathway for the emissive ^{3}MLCT state. Accordingly, these complexes are not emissive at room temperature, while strong emission is seen from 77 K glasses.

$[Re(CNx)(CO)_3(phen')]^+$ (phen′ = Me and Ph-substituted phen) are strongly emissive even at room temperature. TD-DFT calculations have revealed [230] a Re,CNx → phen′ MLLCT character of the lowest allowed singlet transitions. Strongly delocalized transitions closely follow at higher energies. The lowest triplet was identified as Ru,CNx → phen′ ^{3}MLLCT in all complexes. The energy differences from the ground state, calculated at optimized ^{3}MLLCT geometries in EtOH, are only 500–1200 cm^{-1} higher than experimental emission energies measured from 77 K EtOH/MeOH glasses. The lowest ^{3}MLLCT is followed by ^{3}LF or ^{3}IL(phen′) states. Lying at energies higher than 4600 cm^{-1}, they are not thermally accessible and, hence, $[Re(CNx)(CO)_3(phen')]^+$ complexes show strong ^{3}MLCT emission.

$[Re(CNx)_6]^+$ and $[Re(CNx)_5Cl]$ are emissive in low-temperature glasses but not at room temperature [231]. For the former complex, all allowed singlet transitions were assigned as Re,CNx → CNx MLLCT. The KS orbitals involved appear highly delocalized. The situation is more complicated for $[Re(CNx)_5Cl]$, where a series of close-lying Re,CNx → CNx MLLCT transitions is followed by two CNx,Cl → CNx LLCT transitions. Surprisingly, d(π)Re and pπ(Cl) orbitals mix very little. Hence, Re,Cl → CNx MLLCT transitions do not appear to contribute to the spectra. The lowest triplet states are again ^{3}MLLCT, followed in energy by states with ^{3}LF and CNx → CNx LLCT contributions, the latter involving different CNx ligands. Population of these higher states is probably responsible for the fast nonradiative decay at room temperature.

Calculated spectra in all these studies match the experiment remarkably well. However, one can wonder whether some of the contributions from long-range CT, such as CNx → phen′ or CNx,Cl → CNx, are not exaggerated by TD-DFT or UKS.

These studies have interesting implications for our description of bonding in arylisocyanide metal complexes. It follows that the high-lying occupied MOs are delocalized over the CNx ligand, containing only about 50% of the metal contribution, due to a strong π-back donation. This pushes the unoccupied π^* arylisocyanide orbitals up in energy. Consequently, in diimine-arylisocyanide mixed-ligand complexes, the polypyridine (phen′, bpy) is always the site to which the low-lying transitions are directed.

9. Conclusions

DFT techniques provide a remarkably good description of low-lying electronic transitions and excited states of complexes of electron-rich d^6 metals with electron-accepting ligands, usually polypyridines and α-diimines. TD-DFT calculates vertical transitions and well reproduces absorption spectra. It can be used to optimize singlet and triplet excited-state structures, including higher-lying states. Alternatively, the structures of the lowest states of given spin and symmetry can be optimized by a separate DFT calculation, usually UKS. Excited-state properties such as emission, absorption, molecular structure, vibrational frequencies, electron-density and spin-density distribution, *etc*. can then be calculated. TD-DFT and DFT help us to elucidate photochemical mechanisms and photophysical relaxation pathways by calculating energies, characters and properties of spectroscopically silent but photochemically relevant states.

Problems can be encountered for low-symmetry complexes, which contain electron-rich ligands (halides, NCS^- or even styrylpyridine) alongside electron-accepting ligands in their coordination spheres, or electron-rich substituents on a ligand periphery (*e.g.* COO^- on bpy). TD-DFT and DFT tend to underestimate energies of long-range charge transfer from such ligands or groups and overestimate its admixture to more localized, shorter-range CT transitions such as MLCT. On an orbital level, these effects are manifested by an excessive delocalization of high-lying MOs over the electron-rich moieties. These problems can be remedied by using hybrid functionals which include Hartree–Fock exchange (PBE0, B3LYP) and calculating the molecule in the actual solvent, described by an appropriate continuum model. Such calculations yield reliable transition

energies and excited-state descriptions even for complicated CT transitions in mixed-ligand complexes.

Calculations performed on a wide range of carbonyl-diimine complexes, organometallics and coordination compounds of d^6 metals with electron-accepting ligand(s) point to highly mixed characters of low-lying transitions and excited states, which should be described as MLLCT (metal–ligand-to-ligand CT) instead of traditional MLCT, LLCT, *etc*. Excited electron density originates in an extended spatial region of the molecule which includes the metal atom and part of its coordination sphere. The metal and ligand contributions vary with the chromophore structure and the medium. Polar solvents generally favor larger charge separation upon excitation.

Calculations also reveal a large extent of mixing between metal d orbitals and ligand orbitals in carbonyl-diimine complexes. Consequently, the d-character is spread over many more MOs than predicted by the LF theory. Traditional LF arguments are hardly applicable to these complexes. Pure LF (dd) excited states do not occur as such in heavy-metal carbonyl-diimine complexes, but the LF character is admixed into high-lying excited states. Despite their high energies, these states can play role in photochemistry since they interact with lower-lying CT states upon metal–ligand bond elongation.

DFT studies of functional assemblies composed of a transition-metal complex and a nanoparticle or a biomolecule have identified charge-transfer excited states pertinent to the whole assemblies and point to active spectroscopic and photophysical roles of the molecular environment of transition metal chromophores.

Further developments of DFT-techniques are expected to provide even deeper insight and prediction of spectroscopic, photophysical and photochemical phenomena in metal complexes. Much needed are new functionals which would better describe long-range CT and other non-local effects. New applications will require incorporation of spin-orbit coupling into TD-DFT and development of methods to calculate energetically close-lying excited states and avoided crossings of their potential energy curves. Combining DFT and wavefunction techniques could be a promising way forward. Another important problem, which was hardly yet tackled by DFT, is long-range electron transfer in mixed-valence complexes and electron-transfer dyads. Great opportunities exist in calculating large molecular assemblies and metal complexes attached to nanoparticles. Further progress is expected in improving the description of the chromophore environment beyond the continuous models, to treat specific interactions and anisotropic media such as proteins and supramolecular hosts. Finally, coupling TD-DFT calculations with molecular dynamics could provide a new, dynamic, view of excited-state behavior, optically controlled processes and functions of transition-metal chromophores.

Acknowledgments

Support from the COST D35 Action, Ministry of Education of the Czech Republic (Grant no. 1P05OC068) and QMUL is gratefully appreciated.

References

[1] A. Vlček Jr., Coord. Chem. Rev. 200–202 (2000) 933.
[2] A.C. Bhasikuttan, M. Suzuki, S. Nakashima, T. Okada, J. Am. Chem. Soc. 124 (2002) 8398.
[3] A.C. Bhasikuttan, T. Okada, J. Phys. Chem. B 108 (2004) 12629.
[4] Z.A. Siddique, Y. Yamamoto, T. Ohno, K. Nozaki, Inorg. Chem. 42 (2003) 6366.
[5] Z.A. Siddique, T. Ohno, K. Nozaki, Inorg. Chem. 43 (2004) 663.
[6] A. Cannizzo, F. van Mourik, W. Gawelda, G. Zgrablic, C. Bressler, M. Chergui, Angew. Chem. Int. Ed. 45 (2006) 3147.
[7] A. Vlček Jr., I.R. Farrell, D.J. Liard, P. Matousek, M. Towrie, A.W. Parker, D.C. Grills, M.W. George, J. Chem. Soc., Dalton Trans. (2002) 701.
[8] M.K. Kuimova, W.Z. Alsindi, J. Dyer, D.C. Grills, O.S. Jina, P. Matousek, A.W. Parker, P. Portius, X.-Z. Sun, M. Towrie, C. Wilson, J. Yang, M.W. George, Dalton Trans. (2003) 3996.
[9] C.A. Bignozzi, J.R. Schoonover, R.B. Dyer, Commun. Inorg. Chem. 18 (1996) 77.
[10] J.R. Schoonover, G.F. Strouse, Chem. Rev. 98 (1998) 1335.
[11] J. Bredenbeck, J. Helbing, P. Hamm, J. Am. Chem. Soc. 126 (2004) 990.
[12] J. Bredenbeck, J. Helbing, P. Hamm, Phys. Rev. Lett. 95 (2005) 083201.
[13] L.X. Chen, Angew. Chem. Int. Ed. 43 (2004) 2886.
[14] M. Saes, C. Bressler, R. Abela, D. Grolimund, S.L. Johnson, P.A. Heimann, M. Chergui, Phys. Rev. Lett. 90 (2003) 047403.
[15] L.X. Chen, G. Jennings, T. Liu, D.J. Gosztola, J.P. Hessler, D.V. Scaltrito, G.J. Meyer, J. Am. Chem. Soc. 124 (2002) 10861.
[16] L.X. Chen, G.B. Shaw, I. Novozhilova, T. Liu, G. Jennings, K. Attenkofer, G.J. Meyer, P. Coppens, J. Am. Chem. Soc. 125 (2003) 7022.
[17] W. Gawelda, M. Johnson, F.M.F. de Groot, R. Abela, C. Bressler, M. Chergui, J. Am. Chem. Soc. 128 (2006) 5001.
[18] W. Gawelda, M. Johnson, F.M.F. de Groot, R. Abela, C. Bressler, M. Chergui, J. Am. Chem. Soc. 128 (2006) 5001.
[19] D. Shorokhov, S.T. Park, A.H. Zewail, Chem. Phys. Chem. 6 (2005) 2228.
[20] C.H. Martin, M.C. Zerner, in: E.I. Solomon, A.B.P. Lever (Eds.), Inorganic Electronic Structure and Spectroscopy, vol. 1: Methodology, John Wiley & Sons Inc., New York, 1999, p. 555.
[21] R.A. Friesner, Proc. Natl. Acad. Sci. U.S.A. 102 (2005) 6648.
[22] P. Atkins, R. Friedman, Molecular Quantum Mechanics, Oxford University Press, Oxford, 2005.
[23] E.J. Heller, J. Chem. Phys. 62 (1975) 1544.
[24] A. Acosta, J.I. Zink, J. Organomet. Chem. 554 (1998) 87.
[25] J.I. Zink, K.-S. Kim Shin, in: D.H. Volman, G.S. Hammond, D.C. Neckers (Eds.), Advances in Photochemistry, 1991, p. 119.
[26] M.C. Heitz, D. Guillaumont, I. Cote-Bruand, C. Daniel, J. Organomet. Chem. 609 (2000) 66.
[27] C. Daniel, Coord. Chem. Rev. 238/239 (2003) 143.
[28] J. Bossert, N. Ben Amor, A. Strich, C. Daniel, Chem. Phys. Lett. 342 (2001) 617.
[29] D. Guillaumont, C. Daniel, A. Vlček Jr., J. Phys. Chem. A 105 (2001) 1107.
[30] M.C. Heitz, K. Finger, C. Daniel, Coord. Chem. Rev. 159 (1997) 171.
[31] D. Guillaumont, C. Daniel, Coord. Chem. Rev. 177 (1998) 181.
[32] K. Finger, C. Daniel, P. Saalfrank, B. Schmidt, J. Phys. Chem. 100 (1996) 3368.
[33] D. Guillaumont, C. Daniel, J. Am. Chem. Soc. 121 (1999) 11733.
[34] I. Bruand-Cote, C. Daniel, Chem. Eur. J. 8 (2002) 1183.
[35] M.-C. Heitz, C. Daniel, J. Am. Chem. Soc. 119 (1997) 8269.
[36] J. Full, C. Daniel, L. González, Phys. Chem. Chem. Phys. 5 (2003) 87.
[37] C. Daniel, Coord. Chem. Rev. 230 (2002) 65.
[38] J. Simons, An Introduction Theoretical Chemistry, Cambridge University Press, Cambridge, 2003.
[39] N. Ben Amor, S. Villaume, D. Maynau, C. Daniel, Chem. Phys. Lett. 421 (2006) 378.
[40] S.I. Gorelsky, A.B.P. Lever, M. Ebadi, Coord. Chem. Rev. 230 (2002) 97.
[41] R.A. Metcalfe, A.B.P. Lever, Inorg. Chem. 36 (1997) 4762.
[42] A. DelMedico, E.S. Dodsworth, A.B.P. Lever, Inorg. Chem. 43 (2004) 2654.

[43] C.J. da Cunha, E.S. Dodsworth, M.A. Monteiro, A.B.P. Lever, Inorg. Chem. 38 (1999) 5399.
[44] H. Masui, A.L. Freda, M.C. Zerner, A.B.P. Lever, Inorg. Chem. 39 (2000) 141.
[45] T. Renouard, R.-A. Fallahpour, M.K. Nazeeruddin, R. Humphry-Baker, S.I. Gorelsky, A.B.P. Lever, M. Grätzel, Inorg. Chem. 41 (2002) 367.
[46] S.I. Gorelsky, A.B.P. Lever, J. Organomet. Chem. 635 (2001) 187.
[47] M.K. Nazeeruddin, Q. Wang, L. Cevey, V. Aranyos, P. Liska, E. Figgemeier, C. Klein, N. Hirata, S. Koops, S.A. Haque, J.R. Durrant, A. Hagfeldt, A.B.P. Lever, M. Grätzel, Inorg. Chem. 45 (2006) 787.
[48] J. Li, L. Noodleman, D.A. Case, in: E.I. Solomon, A.B.P. Lever (Eds.), Inorganic Electronic Structure and Spectroscopy, John Wiley & Sons Inc., New York, 1999.
[49] W. Koch, M.C. Holthausen, A Chemist's Guide to Density Functional Theory, Wiley/VCH, Weinheim, 2000.
[50] E.J. Baerends, O.V. Gritsenko, J. Phys. Chem. A 101 (1997) 5383.
[51] H. Chermette, Coord. Chem. Rev. 178–180 (1998) 699.
[52] W. Kohn, A.D. Becke, R.G. Parr, J. Phys. Chem. 100 (1996) 12974.
[53] R.G. Parr, W. Yang, Density-Functional Theory of Atoms and Molecules, Oxford University Press, New York, 1989.
[54] A. Dreuw, M. Head-Gordon, Chem. Rev. 105 (2005) 4009.
[55] T. Ziegler, J. Chem. Soc., Dalton Trans. (2002) 642.
[56] R. Stowasser, R. Hoffmann, J. Am. Chem. Soc. 121 (1999) 3414.
[57] M. Turki, C. Daniel, S. Záliš, A. Vlček Jr., J. van Slageren, D.J. Stufkens, J. Am. Chem. Soc. 123 (2001) 11431.
[58] S. Záliš, N. Ben Amor, C. Daniel, Inorg. Chem. 43 (2004) 7978.
[59] A.E. Mattsson, Science 298 (2002) 759.
[60] A.D. Becke, Phys. Rev. A 38 (1988) 3098.
[61] J.P. Perdew, Phys. Rev. A 33 (1986) 8822.
[62] P.R.T. Schipper, O.V. Gritsenko, S.J.A. van Gisbergen, E.J. Baerends, J. Chem. Phys. 112 (2000) 1344.
[63] A. Rosa, G. Ricciardi, O. Gritsenko, E.J. Baerends, Struct. Bond. 112 (2004) 49.
[64] S. Záliš, M. Busby, T. Kotrba, P. Matousek, M. Towrie, A. Vlček Jr., Inorg. Chem. 43 (2004) 1723.
[65] A.D. Becke, J. Chem. Phys. 98 (1993) 5648.
[66] C. Adamo, V. Barone, J. Chem. Phys. 110 (1999) 6158.
[67] J.P. Perdew, K. Burke, M. Ernzerhof, Phys. Rev. Lett. 77 (1996) 3865.
[68] R.K. Szilagyi, M. Metz, E.I. Solomon, J. Phys. Chem. A 106 (2002) 2994.
[69] D. Cremer, Mol. Phys. 99 (2001) 1899.
[70] M. Dierksen, S. Grimme, J. Phys. Chem. A 108 (2004) 10225.
[71] M. Seth, T. Ziegler, J. Chem. Phys. 123 (2005) 144105.
[72] M.-F. Charlot, Y. Pellegrin, A. Quaranta, W. Leibl, A. Aukauloo, Chem. Eur. J. 12 (2006) 796.
[73] E.K.U. Gross, J.F. Dobson, M. Petersilka, Top. Curr. Chem. 181 (1996) 81.
[74] M.E. Casida, in: D.P. Chong (Ed.), Recent Advances in Density-Functional Methods, World Scientific, Singapore, 1995, p. 155.
[75] S.J.A. van Gisbergen, J.A. Groeneveld, A. Rosa, J.G. Snijders, E.J. Baerends, J. Phys. Chem. A 103 (1999) 6835.
[76] J.E. Monat, J.H. Rodriguez, J.K. McCusker, J. Phys. Chem. A 106 (2002) 7399.
[77] J. Neugebauer, E.J. Baerends, M. Nooijen, J. Phys. Chem. A 109 (2005) 1168.
[78] O. Gritsenko, E.J. Baerends, J. Chem. Phys. 121 (2004) 655.
[79] A. Dreuw, M. Head-Gordon, J. Am. Chem. Soc. 126 (2004) 4007.
[80] D.J. Tozer, J. Chem. Phys. 119 (2003) 12697.
[81] A. Dreuw, J.L. Weisman, M. Head-Gordon, J. Chem. Phys. 119 (2003) 2943.
[82] D.J. Tozer, R.D. Amos, N.C. Handy, B.O. Roos, L. Serrano-Andrés, Mol. Phys. 97 (1999) 859.
[83] W. Hieringer, A. Görling, Chem. Phys. Lett. 419 (2006) 557.
[84] J. Bossert, C. Daniel, Chem. Eur. J. 12 (2006) 4835.
[85] M. Busby, P. Matousek, M. Towrie, A. Vlček Jr., J. Phys. Chem. A 109 (2005) 3000.
[86] C. Adamo, V. Barone, Theor. Chem. Acc. 105 (2000) 169.
[87] C. Adamo, G.E. Scuseria, V. Barone, J. Chem. Phys. 111 (1999) 2889.
[88] J.-F. Guillemoles, V. Barone, L. Joubert, C. Adamo, J. Phys. Chem. A 106 (2002) 11354.
[89] R. Kobayashi, R.D. Amos, Chem. Phys. Lett. 420 (2006) 106.
[90] J. Tomasi, B. Mennucci, R. Cammi, Chem. Rev. 105 (2005) 2999.
[91] V. Barone, F. Fabrizi de Biani, E. Ruiz, B. Sieklucka, J. Am. Chem. Soc. 123 (2001) 10742.
[92] C. Adamo, V. Barone, Chem. Phys. Lett. 330 (2000) 152.
[93] E. Goll, H.-J. Werner, H. Stoll, Phys. Chem. Chem. Phys. 7 (2005) 3917.
[94] F. Furche, R. Ahlrichs, J. Chem. Phys. 117 (2002) 7433.
[95] A. Dreuw, B.D. Dunietz, M. Head-Gordon, J. Am. Chem. Soc. 124 (2002) 12070.
[96] B.D. Dunietz, A. Dreuw, M. Head-Gordon, J. Phys. Chem. B 107 (2003) 5623.
[97] T.P.M. Goumans, A.W. Ehlers, M.C. van Hemert, A. Rosa, E.J. Baerends, K. Lammertsma, J. Am. Chem. Soc. 125 (2003) 3558.
[98] A. Bérces, T. Ziegler, Top. Curr. Chem. 182 (1996) 41.
[99] M.W. Wong, Chem. Phys. Lett. 256 (1996) 391.
[100] R.L. Martin, J. Chem. Phys. 118 (2003) 4775.
[101] E.R. Batista, R.L. Martin, J. Phys. Chem. A 109 (2005) 3128.
[102] M. Head-Gordon, A.M. Grańa, D. Maurice, C.A. White, J. Phys. Chem. 99 (1995) 14261.
[103] S. Záliš, I.R. Farrell, A. Vlček Jr., J. Am. Chem. Soc. 125 (2003) 4580.
[104] S. Záliš, C. Daniel, A. Vlček Jr., J. Chem. Soc., Dalton Trans. (1999) 3081.
[105] P. Chen, T.J. Meyer, Chem. Rev. 98 (1998) 1439.
[106] D.J. Stufkens, Coord. Chem. Rev. 104 (1990) 39.
[107] D.J. Stufkens, A. Vlček Jr., Coord. Chem. Rev. 177 (1998) 127.
[108] W. Kaim, S. Kohlmann, S. Ernst, B. Olbrich-Deussner, C. Bessenbacher, A. Schultz, J. Organomet. Chem. 321 (1987) 215.
[109] R.W. Balk, T. Snoeck, D.J. Stufkens, A. Oskam, Inorg. Chem. 19 (1980) 3015.
[110] B.S. Brunschwig, S. Ehrenson, N. Sutin, J. Phys. Chem. 90 (1986) 3657.
[111] A.M. Blanco-Rodríguez, A. Gabrielsson, M. Motevalli, P. Matousek, M. Towrie, J. Šebera, S. Záliš, A. Vlček Jr., J. Phys. Chem. A 109 (2005) 5016.
[112] H.A. Nieuwenhuis, D.J. Stufkens, A. Oskam, Inorg. Chem. 33 (1994) 3212.
[113] B.D. Rossenaar, D.J. Stufkens, A. Vlček Jr., Inorg. Chem. 35 (1996) 2902.
[114] S.R. Stoyanov, J.M. Villegas, D.P. Rillema, Inorg. Chem. Commun. 7 (2004) 838.
[115] P. Hummel, J. Oxgaard, W.A. Goddard III, H.B. Gray, Inorg. Chem. 44 (2005) 2454.
[116] A.J. Vlček, Coord. Chem. Rev. 230 (2002) 225.
[117] A. Gabrielsson, S. Záliš, P. Matousek, M. Towrie, A. Vlček Jr., Inorg. Chem. 43 (2004) 7380.
[118] J. Víchová, F. Hartl, A. Vlček Jr., J. Am. Chem. Soc. 114 (1992) 10903.
[119] I.R. Farrell, P. Matousek, M. Towrie, A.W. Parker, D.C. Grills, M.W. George, A. Vlček Jr., Inorg. Chem. 17 (2002) 4318.
[120] E. Eskelinen, T.-J.J. Kinnunen, M. Haukka, T.A. Pakkanen, Eur. J. Inorg. Chem. (2002) 1169.
[121] S. Luukkanen, M. Haukka, E. Eskelinen, T.A. Pakkanen, V. Lehtovuori, J. Kallioinen, P. Myllyperkiö, J.E.I. Korppi-Tommola, Phys. Chem. Chem. Phys. 3 (2001) 1992.
[122] D.J. Stufkens, Comments Inorg. Chem. 13 (1992) 359.
[123] D.J. Stufkens, M.P. Aarnts, J. Nijhoff, B.D. Rossenaar, A. Vlček Jr., Coord. Chem. Rev. 171 (1998) 93.
[124] D.J. Stufkens, M.P. Aarnts, B.D. Rossenaar, A. Vlček Jr., Pure Appl. Chem. 69 (1997) 831.
[125] L.A. Worl, R. Duesing, P. Chen, L. Della Ciana, T.J. Meyer, J. Chem. Soc., Dalton Trans. (1991) 849.
[126] M.W. George, F.P.A. Johnson, J.R. Westwell, P.M. Hodges, J.J. Turner, J. Chem. Soc., Dalton Trans. (1993) 2977.
[127] K. Kalyanasundaram, J. Chem. Soc., Faraday Trans. 2 82 (1986) 2401.
[128] W.K. Smothers, M.S. Wrighton, J. Am. Chem. Soc. 105 (1983) 1067.
[129] M.S. Wrighton, D.L. Morse, J. Am. Chem. Soc. 96 (1974) 998.
[130] A. Vlček Jr., S. Záliš, J. Phys. Chem. A 109 (2005) 2991.

[131] P.C. Hariharan, J.A. Pople, Theor. Chim. Acta 28 (1973) 213.
[132] D.E. Woon, T.H. Dunning Jr., J. Chem. Phys. 98 (1993) 1358.
[133] D. Andrae, U. Häussermann, M. Dolg, H. Stoll, H. Preuss, Theor. Chim. Acta 77 (1990) 123.
[134] L. Yang, A.-M. Ren, J.K. Feng, X.-J. Liu, Y.-G. Ma, M. Zhang, X.-D. Liu, J.-C. Shen, H.-X. Zhang, J. Phys. Chem. A 108 (2004) 6797.
[135] D.M. Dattelbaum, R.L. Martin, J.R. Schoonover, T.J. Meyer, J. Phys. Chem. A 108 (2004) 3518.
[136] D.M. Dattelbaum, K.M. Omberg, P.J. Hay, N.L. Gebhart, R.L. Martin, J.R. Schoonover, T.J. Meyer, J. Phys. Chem. A 108 (2004) 3527.
[137] D.M. Dattelbaum, K.M. Omberg, J.R. Schoonover, R.L. Martin, T.J. Meyer, Inorg. Chem. 41 (2002) 6071.
[138] D.J. Liard, M. Busby, P. Matousek, M. Towrie, A. Vlček Jr., J. Phys. Chem. A 108 (2004) 2363.
[139] G.J. Stor, D.J. Stufkens, A. Oskam, Inorg. Chem. 31 (1992) 1318.
[140] H.A. Nieuwenhuis, D.J. Stufkens, R.-A. McNicholl, A.H.R. Al-Obaidi, C.G. Coates, S.E.J. Bell, J.J. McGarvey, J. Westwell, M.W. George, J.J. Turner, J. Am. Chem. Soc. 117 (1995) 5579.
[141] H.A. Nieuwenhuis, D.J. Stufkens, A. Oskam, A. Vlček Jr., Inorg. Chem. 34 (1995) 3879.
[142] J. Bredenbeck, P. Hamm, A.M. Blanco-Rodríguez, S. Záliš, A. Vlček Jr., in preparation.
[143] D.J. Stufkens, A. Vlček Jr., The Spectrum 9 (1996) 2.
[144] A. Basu, M.A. Weiner, T.C. Strekas, H.D. Gafney, Inorg. Chem. 21 (1982) 1085.
[145] A. Juris, S. Campagna, I. Bidd, J.-M. Lehn, R. Ziessel, Inorg. Chem. 27 (1988) 4007.
[146] J.K. Hino, L. Della Ciana, W.J. Dressick, B.P. Sullivan, Inorg. Chem. 31 (1992) 1072.
[147] D.M. Manuta, A.J. Lees, Inorg. Chem. 25 (1986) 1354.
[148] M. Busby, P. Matousek, M. Towrie, A.J. Di Bilio, H.B. Gray, A.J. Vlček, Inorg. Chem. 43 (2004) 4994.
[149] A. Gabrielsson, P. Matousek, M. Towrie, F. Hartl, S. Záliš, A. Vlček Jr., J. Phys. Chem. A 109 (2005) 6147.
[150] M.-N. Collomb-Dunand-Sauthier, A. Deronzier, R. Ziessel, J. Organomet. Chem. 444 (1993) 191.
[151] E. Eskelinen, M. Haukka, T. Venäläinen, T.A. Pakkanen, M. Wasberg, S. Chardon-Noblat, A. Deronzier, Organometallics 19 (2000) 163.
[152] V. Lehtovuori, J. Kallioinen, P. Myllyperkiö, M. Haukka, J. Korpi-Tommola, Chem. Phys. 295 (2003) 81.
[153] A. Vlček Jr., Coord. Chem. Rev. 177 (1998) 219.
[154] A. Vlček Jr., J. Víchová, F. Hartl, Coord. Chem. Rev. 132 (1994) 167.
[155] D. Guillaumont, C. Daniel, A. Vlček Jr., Inorg. Chem. 36 (1997) 1684.
[156] C. Pollak, A. Rosa, E.J. Baerends, J. Am. Chem. Soc. 119 (1997) 7324.
[157] E.J. Baerends, A. Rosa, Coord. Chem. Rev. 177 (1998) 97.
[158] G.L. Geoffroy, M.S. Wrighton, Organometallic Photochemistry, Academic Press, New York, 1979.
[159] A.J. Lees, Chem. Rev. 87 (1987) 711.
[160] N.A. Beach, H.B. Gray, J. Am. Chem. Soc. 90 (1968) 5713.
[161] K. Pierloot, E. Tsokos, L.G. Vanquickenborne, J. Phys. Chem. 100 (1996) 16545.
[162] A. Rosa, E.J. Baerends, S.J.A. van Gisbergen, E. van Lenthe, J.A. Groeneveld, J.G. Snijders, J. Am. Chem. Soc. 121 (1999) 10356.
[163] T. Lian, S.E. Bromberg, M.C. Asplund, H. Yang, C.B. Harris, J. Phys. Chem. 100 (1996) 11994.
[164] M.J. Patterson, P.A. Hunt, M.A. Robb, O. Takahashi, J. Phys. Chem. A 106 (2002) 10494.
[165] R.S. Panesar, N. Dunwoody, A.J. Lees, Inorg. Chem. 37 (1998) 1648.
[166] S. Záliš, A. Vlček Jr., C. Daniel, Coll. Czechoslov. Chem. Commun. 68 (2003) 89.
[167] K.A. Rawlins, A.J. Lees, A.W. Adamson, Inorg. Chem. 29 (1990) 3866.
[168] F.P.A. Johnson, M.W. George, S.L. Morrison, J.J. Turner, J. Chem. Soc., Chem. Commun. (1995) 391.
[169] P. Glyn, F.P.A. Johnson, M.W. George, A.J. Lees, J.J. Turner, Inorg. Chem. 30 (1991) 3543.
[170] I.R. Farrell, F. Hartl, S. Záliš, T. Mahabiersing, A. Vlček Jr., J. Chem. Soc., Dalton Trans. (2000) 4323.
[171] I.R. Farrell, J. van Slageren, S. Záliš, A. Vlček Jr., Inorg. Chim. Acta 315 (2001) 44.
[172] I. Veroni, C. Makedonas, A. Rontoyianni, C.A. Mitsopoulou, J. Organomet. Chem. 691 (2005) 267.
[173] I.R. Farrell, P. Matousek, A. Vlček Jr., J. Am. Chem. Soc. 121 (1999) 5296.
[174] I.G. Virrels, M.W. George, J.J. Turner, J. Peters, A. Vlček Jr., Organometallics 15 (1996) 4089.
[175] A.J. Lees, J. Organomet. Chem. 554 (1998) 1.
[176] N. Dunwoody, A.J. Lees, Organometallics 16 (1997) 5770.
[177] S.E. Bromberg, H. Yang, M.C. Asplund, T. Lian, B.K. McNamara, K.T. Kotz, J.S. Yeston, M. Wilkens, H. Frei, R.G. Bergman, C.B. Harris, Science 278 (1997) 260.
[178] T. Lian, S.E. Bromberg, H. Yang, G. Proulx, R.G. Bergman, C.B. Harris, J. Am. Chem. Soc. 118 (1996) 3769.
[179] S.E. Bromberg, T. Lian, R.G. Bergman, C.B. Harris, J. Am. Chem. Soc. 118 (1996) 2069.
[180] Z. Hu, R.J. Boyd, H. Nakatsuji, J. Am. Chem. Soc. 124 (2002) 2664.
[181] K. Finger, C. Daniel, J. Am. Chem. Soc. 117 (1995) 12322.
[182] D. Guillaumont, M.P. Wilms, C. Daniel, D.J. Stufkens, Inorg. Chem. 37 (1998) 5816.
[183] C. Daniel, D. Guillaumont, C. Ribbing, B. Minaev, J. Phys. Chem. A 103 (1999) 5766.
[184] D. Guillaumont, K. Finger, M.R. Hachey, C. Daniel, Coord. Chem. Rev. 171 (1998) 439.
[185] M. Turki, C. Daniel, Coord. Chem. Rev. 216–217 (2001) 31.
[186] M.R.J. Hachey, C. Daniel, Inorg. Chem. 37 (1998) 1387.
[187] V. Vallet, J. Bossert, A. Strich, C. Daniel, Phys. Chem. Chem. Phys. 5 (2003) 2948.
[188] V. Vallet, A. Strich, C. Daniel, Chem. Phys. 311 (2005) 13.
[189] C. Daniel, J. Full, L. González, C. Lupulescu, J. Manz, A. Merli, Š. Vajda, L. Wöste, Science 299 (2003) 536.
[190] J. Brooks, Y. Babayan, S. Lamansky, P.I. Djurovich, I. Tsyba, R. Bau, M.E. Thompson, Inorg. Chem. 41 (2002) 3055.
[191] P.J. Hay, J. Phys. Chem. A 106 (2002) 1634.
[192] M.S. Lowry, W.R. Hudson, R.A. Pascal Jr., S. Bernhard, J. Am. Chem. Soc. 126 (2004) 14129.
[193] L. Ghizdavu, O. Lentzen, S. Schumm, A. Brodkorb, C. Moucheron, A. Kirsch-De Mesmaeker, Inorg. Chem. 42 (2003) 1935.
[194] M. Polson, M. Ravaglia, S. Fracasso, M. Garavelli, F. Scandola, Inorg. Chem. 44 (2005) 1282.
[195] A.B. Tamayo, S. Garon, T. Sajoto, P.I. Djurovich, I.M. Tsyba, R. Bau, M.E. Thompson, Inorg. Chem. 44 (2005) 8723.
[196] J.-K. Yu, Y.-M. Cheng, Y.-H. Hu, P.-T. Chou, Y.-L. Chen, S.-W. Lee, Y. Chi, J. Phys. Chem. B 108 (2004) 19908.
[197] Y.-L. Chen, S.-W. Lee, Y. Chi, K.-C. Hwang, S.B. Kumar, Y.-H. Hu, Y.-M. Cheng, P.-T. Chou, S.M. Peng, G.H. Lee, S.J. Yeh, C.-T. Chen, Inorg. Chem. 44 (2005) 4287.
[198] Y.-L. Chen, S.-W. Li, Y. Chi, Y.-M. Cheng, S.-C. Pu, Y.-S. Yeh, P.T. Chou, Chem. Phys. Chem. 6 (2005) 2012.
[199] A.B. Tamayo, B.D. Alleyne, P.I. Djurovich, S. Lamansky, I. Tsyba, N.N. Ho, R. Bau, M.E. Thompson, J. Am. Chem. Soc. 125 (2003) 7377.
[200] M.S. Lowry, J.I. Goldsmith, J.D. Slinker, R. Rohl, R.A. Pascal Jr., G.G. Malliaras, S. Bernhard, Chem. Mater. 17 (2005) 5712.
[201] M.G. Colombo, A. Hauser, H.U. Güdel, Inorg. Chem. 32 (1993) 3088.
[202] K. Pierloot, A. Ceulemans, M. Merchán, L. Serrano-Andrés, J. Phys. Chem. A 104 (2000) 4374.
[203] B. O'Regan, M. Grätzel, Nature 353 (1991) 737.
[204] A. Hagfeldt, M. Grätzel, Acc. Chem. Res. 33 (2000) 269.
[205] M. Grätzel, Coord. Chem. Rev. 111 (1991) 167.
[206] M. Grätzel, J. Photochem. Photobiol. A: Chem. 164 (2004) 3.
[207] M. Grätzel, Nature 414 (2001) 338.
[208] M. Zukalová, A. Zukal, L. Kavan, M.K. Nazeeruddin, P. Liska, M. Grätzel, Nano Lett. 5 (2005) 1789.
[209] S. Fantacci, F. De Angelis, A. Selloni, J. Am. Chem. Soc. 125 (2003) 4381.
[210] F. De Angelis, S. Fantacci, A. Selloni, Chem. Phys. Lett. 389 (2004) 204.

[211] F. De Angelis, S. Fantacci, A. Selloni, M.K. Nazeeruddin, Chem. Phys. Lett. 415 (2005) 115.
[212] M.K. Nazeeruddin, F. De Angelis, S. Fantacci, A. Selloni, G. Viscardi, P. Liska, S. Ito, B. Takeru, M. Grätzel, J. Am. Chem. Soc. 127 (2005) 16835.
[213] P. Persson, M.J. Lundqvist, J. Phys. Chem. B 109 (2005) 11918.
[214] F. De Angelis, A. Tilocca, A. Selloni, J. Am. Chem. Soc. 126 (2004) 15024.
[215] R. Car, M. Parrinello, Phys. Rev. Lett. 55 (1985) 2471.
[216] S.G. Abuabara, L.G.C. Rego, V.S. Batista, J. Am. Chem. Soc. 127 (2005) 18234.
[217] C. Daul, E.J. Baerends, P. Vernooijs, Inorg. Chem. 33 (1994) 3538.
[218] M. Buchs, C. Daul, Chimia 52 (1998) 163.
[219] J. Van Houten, R.J. Watts, Inorg. Chem. 17 (1978) 3381.
[220] P.S. Braterman, A. Harriman, G.A. Heath, L.J. Yellowlees, J. Chem. Soc., Dalton Trans. (1983) 1801.
[221] B.L. Guennic, W. Hieringer, A. Görling, J. Autschbach, J. Phys. Chem. A 109 (2005) 4836.
[222] Y. Pellegrin, A. Quaranta, P. Dorlet, M.-F. Charlot, W. Leibl, A. Aukauloo, Chem. Eur. J. 11 (2005) 3698.
[223] S. Flores-Torres, G.R. Hutchison, L.J. Soltzberg, H.D. Abruña, J. Am. Chem. Soc. 128 (2006) 1513.
[224] S. Fantacci, F. De Angelis, J. Wang, S. Bernhard, A. Selloni, J. Am. Chem. Soc. 126 (2004) 9715.
[225] S. Fantacci, F. De Angelis, A. Sgamellotti, N. Re, Chem. Phys. Lett. 396 (2004) 43.
[226] S. Fantacci, F. De Angelis, A. Sgamellotti, A. Marrone, N. Re, J. Am. Chem. Soc. 127 (2005) 14144.
[227] S.L. Howel, K.C. Gordon, J.J. McGarvey, J. Phys. Chem. A 109 (2005) 2948.
[228] P.J. Walsh, K.C. Gordon, N.J. Lundin, A.G. Blackman, J. Phys. Chem. A 109 (2005) 5933.
[229] J.M. Villegas, S.R. Stoyanov, W. Huang, L.L. Lockyear, J.H. Reibenspies, D.P. Rillema, Inorg. Chem. 43 (2004) 6383.
[230] J.M. Villegas, S.R. Stoyanov, W. Huang, D.P. Rillema, Dalton (2005) 1042.
[231] J.M. Villegas, S.R. Stoyanov, J.H. Reibenspies, D.P. Rillema, Organometallics 24 (2005) 395.